1st AIAA Atmospheric and Space Environments Conference
22 - 25 June 2009, San Antonio, Texas

AIAA 2009-4261

Aerodynamic Simulation of Runback Ice Accretion

Andy P. Broeren*
NASA Glenn Research Center, Cleveland, Ohio 44135

Edward A. Whalen†
The Boeing Company, St. Louis, Missouri 63166

Greg T. Busch‡ and Michael B. Bragg§
University of Illinois, Urbana, Illinois 61801

This paper presents the results of recent investigations into the aerodynamics of simulated runback ice accretion on airfoils. Aerodynamic testing was performed on a full-scale, 72-inch (1828.8-mm) chord, NACA 23012 airfoil model over a Reynolds number range of 4.7×10^6 to 16.0×10^6 and a Mach number range of 0.10 to 0.28. A high-fidelity, ice casting simulation of a runback ice accretion was attached to the model leading edge. For $Re = 16.0\times10^6$ and $M = 0.20$, the artificial ice shape decreased the maximum lift coefficient from 1.82 to 1.51 and decreased the stalling angle of attack from 18.1 deg. to 15.0 deg. In general, the performance effects were insensitive to Reynolds and Mach number changes over the range tested. Aerodynamic testing was also conducted on a quarter-scale, NACA 23012 model (18-inch (457.2-mm) chord) at $Re = 1.8\times10^6$ and $M = 0.18$, using low-fidelity, geometrically-scaled simulations of the full-scale casting. It was found that simple, two-dimensional simulations of the upper and lower surface runback ridges provided the best representation of the full-scale, high-Reynolds number iced-airfoil aerodynamics. Higher-fidelity simulations of the runback ice accretion that included geometrically scaled three-dimensional features resulted in larger performance degradations than what was measured on the full-scale model. Based upon this research, a new subclassification of spanwise-ridge ice is proposed that distinguishes between short and tall ridges. This distinction is made in terms of the fundamental aerodynamic characteristics as described in this paper.

Nomenclature

α	=	airfoil angle of attack
α_{stall}	=	stalling angle of attack, coincident with $C_{l,max}$
c	=	airfoil chord length
C_d	=	drag coefficient
$\Delta C_{d,rms}$	=	percent root-mean-square (RMS) difference in C_d
C_l	=	lift coefficient
$C_{l,\alpha}$	=	lift-curve slope
$C_{l,max}$	=	maximum lift coefficient, coincident with α_{stall}
C_m	=	quarter-chord pitching-moment coefficient
k	=	ice-roughness height or thickness
M	=	freestream Mach number
n	=	wall-normal distance above airfoil surface
Re	=	reynolds number based on chord
u_{RMS}	=	root-mean-square of fluctuating streamwise velocity
U	=	mean streamwise velocity

* Aerospace Engineer, Icing Branch, MS 11-2, 210000 Brookpark Rd., Cleveland, OH 44135, Associate Fellow AIAA.
† Engineer, Member AIAA.
‡ Graduate Research Assistant, Dept. of Aerospace Engineering, Member AIAA.
§ Professor of Aerospace Engineering and Executive Associate Dean for Academic Affairs, Fellow AIAA.

U_∞ = free-stream velocity
x = chordwise position along airfoil
y = normal position from airfoil chord line

I. Introduction

MANY aircraft certified for flight in icing conditions employ anti-icing systems on wing and empennage leading edges, as well as engine nacelles and other aerodynamic surfaces. In some cases, these ice-protection systems allow some fraction of the impinging water to flow downstream from the protected region and freeze, leaving a ridge-type ice accretion. Understanding the aerodynamic effects associated with runback icing is important to ensuring safety of flight operations and reducing development and certification costs. It is difficult and expensive to document the aerodynamic effect of ice accretion in natural icing conditions. Therefore, artificial ice simulations are often used to represent an ice accretion in a wind tunnel, sometimes on a subscale model at lower-than-flight Reynolds number. Subsequent questions naturally arise regarding the fidelity of the simulated ice accretion and Reynolds number effects.

Many of these same issues surround iced-airfoil aerodynamics in general and have recently been addressed in the "Airfoil Ice Accretion Aerodynamics Simulation" research program sponsored by NASA and ONERA.[1] This program quantified many of the uncertainties associated with various subscale simulation methods developed to capture the essential aerodynamic features of the full-scale iced airfoil. The authors considered four types of ice accretion classified by their unique aerodynamics: roughness, streamwise ice, horn ice and spanwise-ridge ice. The aerodynamic characteristics of the spanwise-ridge ice accretion were developed from research related to large ice accretions downstream of protected surfaces typically formed in super-cooled, large-droplet (SLD) conditions. These may be thought of as "tall" spanwise ridges, such that the flowfield is characterized by a large separation bubble aft of the ridge. This leads to significant airfoil performance penalties, often surpassing that of horn ice. However, as will be shown in this article, runback ridges do not usually exhibit this type of flowfield. Spanwise ridges resulting from anti-icing systems tend to be shorter in height above the airfoil surface, cover a larger surface length and have a more streamlined geometry. They may be thought of as "short" due to their reduced impact on the iced-airfoil aerodynamics. Regardless of ice-accretion mechanism, the aerodynamics of "tall" and "short" ridges are significantly different, thus leading to a subclassification of spanwise-ridge ice. Bragg et al.[2] allude to this case in their review of iced-airfoil aerodynamics. This comparison is covered in more detail in this paper.

Aerodynamic performance data for runback ice accretion (or any high-fidelity simulation) on airfoils or wings are scarce in the public domain. Gray and von Glahn[3] documented the associated drag increases due to runback ice accretion in an icing wind tunnel, but were unable to conduct these and other performance measurements over a significant angle of attack range. Calay et al.[4] simulated runback ice accretion ridges using a step, a ramp and a triangular shape, each with a normalized height, k/c = 0.0035 on a NACA 0012 airfoil at $Re = 1.25\times10^6$ and M = 0.08. They found that the drag coefficient at 0-deg. angle of attack increased by up to approximately 0.011 while maximum lift coefficient decreased by up to 0.35 with the shapes at x/c = 0.05. Calay et al.[4] also found that the same artificial ice shapes when located at x/c = 0.15 increased $C_{l,max}$ of the airfoil. The greatest $C_{l,max}$ increase was approximately 0.08 and α_{stall} was delayed by 1 deg. The authors noted that the stall of the airfoil with the ice simulations began from the artificial ice shapes rather than from the trailing edge, as was the case for the clean airfoil. The increase in $C_{l,max}$ was attributed to the flow remaining attached at greater angles of attack than in the clean case. The mechanism by which this occurred was not discussed except to say that the shape added "extra turbulence." Calay et al.[4] concluded that small changes in the artificial ice shapes were able to produce large changes in performance effects thus requiring accurate simulations to properly estimate aerodynamic effects. Papadakis and Gile-Laflin[5] also observed performance increases near maximum lift due to a backward facing ramp with k/c = 0.0041 at x/c = 0.15 and a spoiler with k/c = 0.0053 at x/c = 0.15. Their tests were conducted using a modified NACA 63_A-213 airfoil at $Re = 2.0\times10^6$ and M = 0.17. The ramp increased $C_{l,max}$ by 0.11 and delayed stall by 4 deg. while the spoiler increased $C_{l,max}$ by 0.01 and delayed stall by 1 deg. Tests with the ramp farther forward on the airfoil, at x/c = 0.025 reduced $C_{l,max}$ by 0.23 and the stalling angle of attack by 2 deg. These reports indicate mixed results in performance for simulated runback ridges. Relative to the clean, or uniced airfoil, increases in drag were always observed. However, these artificial ice shapes increased the maximum lift coefficient and stalling angle of attack in some cases. Such increases run contrary to the recent body of research associated with tall, SLD-type spanwise ridge ice accretion.[6-8]

Whalen et al.[9,10] investigated the aerodynamic performance penalties of scaled, runback-type ice accretions on NACA 23012 and NACA 3415 airfoils at $Re = 1.8\times10^6$ and M = 0.18. The performance penalties associated with simple, two-dimensional simulations of runback ice accretion did not agree well with higher-fidelity simulations that

included roughness and a more accurate ice-shape profile. Both simulations were geometrically scaled based upon the ratio of the chord length of the aerodynamic model to that of the icing model. Results similar to the aforementioned studies[4,5] were observed. A simple, square-cylinder simulation (k/c = 0.0035) caused an increase in maximum lift and stalling angle-of-attack for the NACA 3415 airfoil and had a negligible effect on the maximum lift and stalling angle-of-attack of the NACA 23012. Further investigation revealed that this simulation was similar in height to the boundary-layer thickness. The source of this performance effect was linked to the shape's ability to generate a mixing layer that entrained higher-momentum fluid into the boundary layer while generating a small, stable separation bubble. The effect was more pronounced in the case of the NACA 3415 because it exhibits a trailing-edge stall, unlike the NACA 23012 which stalls from the leading edge at the test Reynolds number. Trailing-edge stall can be effectively mitigated by increasing the momentum in the airfoil boundary layer.[9]

The effects observed for the runback-ridge simulations aroused suspicion as to the appropriate method for developing subscale simulations. Geometric scaling had been used in the past with good success.[8,11] Busch et al.,[12] in particular, provide quantitative assessment of ice accretion simulation methods on a quarter-scale model at low-Reynolds number. The lift performance increases due to the 2-D simulations observed by Whalen et al.[9,10] were, in general, not expected and did not agree with the results for higher-fidelity simulations. Because the simulations were similar in height to the local boundary-layer thickness it was theorized that the boundary-layer thickness may be the appropriate length scale. Tests conducted by Whalen et al.[9,10] using two-dimensional boundary-layer-scaled simulations, which were approximately twice as tall as the geometrically-scaled simulations, showed significant penalties that were in better agreement with (geometrically-scaled) higher-fidelity simulations of warm-hold runback ice accretion. However, without aerodynamic performance results at full-scale Reynolds number, it was difficult to draw a definitive conclusion concerning the scaling of these shapes. Lee et al.[13] investigated geometry and Reynolds number scaling of a runback ice accretion on a business-jet wing. They found that geometric scaling did not reproduce the aerodynamics of the full-scale wing with the runback-type spanwise ridge. Empirical methods were used to develop "aerodynamically equivalent" shapes that represented the full-scale, iced-wing aerodynamics on the subscale wing. Reynolds number effects were also found to be significant for this ice shape, unlike the case of the large, leading-edge ice shape that was also tested.

These recent results from subscale model testing at lower-than-flight Reynolds number clearly show the need for high-fidelity, high-Reynolds number aerodynamic data. Therefore a key objective of this work was to determine the effect of a high-fidelity runback ice accretion simulation on airfoil aerodynamic performance at near-flight Reynolds number and quantify the Reynolds number effects. In addition, follow-on subscale testing was conducted with low-fidelity simulations at low-Reynolds number to provide information about the accuracy of aerodynamic simulation methods for the small runback ice accretion. The first objective was achieved by conducting aerodynamic performance testing at the ONERA F1 pressurized wind-tunnel using a 72-inch (1828.8-mm) chord NACA 23012 airfoil over a Reynolds number range of 4.7×10^6 to 16.0×10^6 and a Mach number range of 0.10 to 0.28. The second objective was achieved by conducting aerodynamic performance testing in the University of Illinois low-speed wind-tunnel using an 18-inch (457.2-mm) chord NACA 23012 airfoil at a Reynolds number of 1.8×10^6 and a Mach number of 0.18. Subscale simulations of the runback ice accretion, fabricated using simple-geometric shapes and roughness, were tested on the airfoil for comparison to the full-scale results. Finally, these results were used to further define the aerodynamic characteristics of spanwise-ridge ice. A subclassification is proposed that distinguishes between "tall" and "short" spanwise ridges based upon their respective aerodynamic effects.

II. Experimental Methods

A. F1 Wind Tunnel and Model

The full-scale aerodynamic testing was performed at the ONERA F1 pressurized wind-tunnel facility.[14] The closed-return wind tunnel has a test-section measuring 138-inches (3500-mm) high by 177-inches (4500-mm) wide by 433-inches (11000-mm) long. The maximum test section Mach number is 0.36 and the maximum stagnation pressure is 57 psia (3.85 bar). The unit Reynolds number can be varied up to a maximum of 6.0×10^6/ft at Mach = 0.23. Total temperature is maintained via a heat exchanger located in the second diffuser downstream of the fan. The fan operates at constant speed while the test section Mach number is controlled by adjusting the pitch of the blades. The test-section inlet flow is conditioned through a 7.18-to-1 contraction containing honeycomb flow straightener and three turbulence reduction screens.

The 72-inch (1828.8-mm) chord NACA 23012 airfoil model was mounted vertically in the test section as shown in Fig. 1. The model span was 137.48-inches (3492-mm) and was mounted in the floor force balance. Small gaps between the bottom of the model and the test-section floor as well as the top of the model and the test-section ceiling

were maintained so as not to cause mechanical hysteresis in the force-balance measurements. The model had a main chordwise row of 72 pressure taps located at 43% span measured from the test-section floor. In addition, there was a row of 20 taps oriented spanwise at $x/c = 0.70$ on the upper surface. The model was designed and built with full-span removable, interchangeable leading-edge sections. The baseline leading edge had the clean NACA 23012 profile, while the alternate leading edge had a truncated nose geometry. The latter design facilitated mounting of the runback-ridge ice casting simulation. Accommodations were also made in the pressure tapping to allow for rapid connection of pressure instrumentation in the cast ice shapes. Also shown in Fig. 1 is the wake rake located one chord length downstream of the model trailing edge. The wake rake had 100 stagnation pressure probes spaced 0.79-inch (20-mm) apart and was located at a fixed spanwise station at 57% span above the test-section floor.

Fig. 1 Photograph of full-scale NACA 23012 airfoil model installed in ONERA F1 wind-tunnel test section.

Data acquisition runs were performed in angle of attack sweeps for increasing and then decreasing angle of attack at a constant sweep rate of 0.1 deg./sec. Data were also acquired at fixed angle of attack for selected angles over the range of the sweep and repeat runs were performed. The data shown in this paper are for increasing angle of attack sweeps and have been averaged to the nearest 0.5 deg. in post-processing. During the sweeps, data were acquired from analog transducers in the force balance and for tunnel conditions. The model surface, test-section sidewall, and wake-rake pressures were acquired using an electronically scanned pressure system. The acquisition of these data were synchronized in time corresponding to the angle of attack sweep rate. Lift and pitching-moment coefficients were calculated from the force balance and from the integration of the surface pressure measurements. Good agreement between the integrated-pressure data and the force-balance data were obtained. In this paper, the lift and pitching moment data reported for the clean configuration were obtained from the surface pressures while the data reported for the iced configuration were obtained from the force balance. The force balance data are reported because, in many cases, the stall of the iced-airfoil configurations was characterized by unsteady flow. The available signal conditioning for the force-balance data allowed for more effective filtering of these unsteady effects. Drag coefficient was calculated from the wake pressures using standard momentum-deficit methods and these values are reported in this paper for all configurations. The performance coefficients were corrected for wind-tunnel wall effects using the methods of Allen and Vincenti.[15] The angle of attack sweeps were performed for a large range of Reynolds numbers and Mach numbers as shown in Table 1. The matrix was designed to isolate the independent effects of these parameters. Therefore, Reynolds number variations were performed at Mach numbers of 0.10 and 0.20 while a Mach number variation was performed at a nominal Reynolds number of 12.2×10^6.

Table 1 Matrix of Reynolds and Mach Number Conditions.

	Mach Number		
Reynolds Number	0.10	0.20	0.28
4.7×10^6	X		
8.8×10^6	X	X	
12.2×10^6	X	X	X
16.0×10^6		X	

The experimental uncertainty in the performance coefficients was estimated using the methods of Kline and McClintock[16] and Coleman and Steele[17] for 20:1 odds. Table 2 lists these uncertainties for both integrated-pressure and force-balance measurements, before the wall corrections were applied. The values were calculated based upon the clean model configuration at $Re = 8.1\times10^6$ and $M = 0.20$. The uncertainties are expected to be identical for the iced-model configurations. The absolute uncertainties in Table 2 are inversely proportional to the dynamic pressure (except for α). This condition was selected because it corresponds to the average dynamic pressure over the range of conditions (cf. Table 1). Therefore, conditions having lower dynamic pressure would have slightly larger uncertainties while conditions with higher dynamic pressure would have slightly lower uncertainties. All of these uncertainties were acceptable for the purposes of this investigation. The relative uncertainty in C_m (both pressure and balance) seems large for this example because of the small reference value. For cases where the C_m values were larger, e.g. in the iced-airfoil case, the absolute uncertainty would be similar, therefore resulting in a

lower relative uncertainty. This is also the case for the uncertainty in drag coefficient. Finally, several repeat runs were performed for both clean and iced configurations and these run-to-run variations in the coefficients were much smaller than the uncertainties listed in Table 2.

Table 2 Estimated Experimental Uncertainties for Measurements in the ONERA F1 Wind Tunnel.

Aerodynamic Quantity	Reference Value	Absolute Uncertainty	Relative Uncertainty
α	8.01 deg.	±0.02 deg.	±0.25%
C_l Balance	1.095	±0.010	±0.93%
C_m Balance	-0.0144	±0.00071	±4.9%
C_p	-1.057	±0.032	±3.05%
C_l Pressure	1.096	±0.0070	±0.64%
C_m Pressure	-0.0148	±0.0024	±16.5%
C_d Wake	0.0086	±0.00048	±5.5%

B. Illinois Wind Tunnel and Model

The subscale aerodynamic testing was conducted in the University of Illinois subsonic, low-turbulence, open-return wind tunnel, which had a test section measuring 33.63-inches (853-mm) high, 48-inches (1219-mm) wide, and 96-inches (2438-mm) long. The testing was performed on an aluminum NACA 23012 airfoil model having a chord length of 18-inches (457.2-mm) and a span of 33.563-inches (852.5-mm). The model had a primary chordwise row of 73 pressure taps located at 51% span. Lift and pitching moment coefficient data were acquired from a force balance and by integration of airfoil surface pressures measured by an electronically scanned pressure system. Excellent agreement between these methods was obtained for the clean model configuration. For the iced configurations, the ice simulations used in this study were not instrumented with pressure taps. This resulted in minor disagreement in the integrated coefficients with the force balance. Therefore, the lift and pitching moment data shown in this paper were obtained from the force balance. Using standard momentum-deficit methods, the drag coefficient was computed from total pressure measurements collected by a traversable wake rake. This wake rake is shown installed behind the airfoil model in Fig. 2. Busch[18] and Blumenthal[19] describe the experimental set-up in greater detail. Experimental uncertainties were calculated using the methods of Kline and McClintock[16] and Coleman and Steele,[17] and a summary of these uncertainties is given in Table 3. While the relative uncertainty of C_m appears to be large because the reference value is small, the absolute uncertainty is reasonable. The angle of attack, lift, pitching-moment and drag coefficients were corrected for wind-tunnel wall boundary effects using the methods of Allen and Vincenti.[15] All data were collected at a Reynolds number of 1.8×10^6 and a Mach number of 0.18, unless noted otherwise.

Fig. 2 Photograph of subscale NACA 23012 airfoil model installed in Illinois wind-tunnel test section.

Table 3 Estimated Experimental Uncertainties for Measurements in the Illinois Wind Tunnel.

Aerodynamic Quantity	Reference Value	Absolute Uncertainty	Relative Uncertainty
α	4.13 deg.	±0.02 deg.	±0.48%
C_l Balance	0.556	±0.00086	±0.16%
C_m Balance	-0.0015	±0.00027	±17.4%
C_p	-0.962	±0.0045	±0.47%
C_d Wake	0.0071	±0.00014	±1.9%

C. Full-scale Model Ice-Shape Simulation Methods

The runback ice simulation tested on the full-scale model was a high-fidelity ice casting that was adapted from an earlier icing test conducted at the NASA Glenn Icing Research Tunnel (IRT).[20,21] The runback ice accretion designated NG0671 was considered to be representative of flight in holding conditions for a full-scale aircraft equipped with a bleed-air, thermal ice-protection system. A mold and casting of this ice accretion were produced and pictures of the completed casting are shown in Fig. 3. Due to the operation of the thermal ice protection system, the leading edge is completely free of ice up to about $x/c = 0.13$ on the upper surface and $x/c = 0.15$ on the lower surface. Characteristics of the upper-surface ridge are that it was continuous along the span, had significant chordwise extent and had some variation in height along the span. In contrast, the lower-surface ridge had a

significant amount of spanwise variation with the largest ice elements being isolated, three-dimensional features, instead of forming a continuous ridge. As discussed in the Introduction, the three-dimensional nature of this type of accretion requires high-fidelity simulation in order to obtain accurate aerodynamic results.

Since the IRT model used to generate ice accretion NG0671 was not identical to the full-scale NACA 23012 model used for the aerodynamic testing, the ice casting was modified to the latter geometry. The castings of the ice ridges shown in Fig. 3 were extracted from the IRT model geometry and applied to a leading edge section corresponding to the full-scale NACA 23012 aerodynamic model. This representation of the runback ice accretion was then used to generate a series of ice-casting sections used for the aerodynamic testing through a process described in detail by Broeren et al.[22] The completed installation is shown in Fig. 4. A tracing of the completed ice shape on the NACA 23012 airfoil leading edge along with the pressure tap locations is given in Fig. 5. This tracing does not show the height profile of the large, isolated ice elements on the lower surface due to a spanwise shift in the tracing location. More details about the ice accretion geometry can be found in Broeren et al.[23] The tracing in Fig. 5 only extends to $x/c = 0.20$ since this was the physical limit of the ice casting section applied to the full-scale NACA 23012 aerodynamic model. Any runback ice downstream of $x/c = 0.20$ was not present in the casting simulation used for aerodynamic testing. This amounted to a very small amount of ice and was considered negligible in terms of its attendant aerodynamic effect.

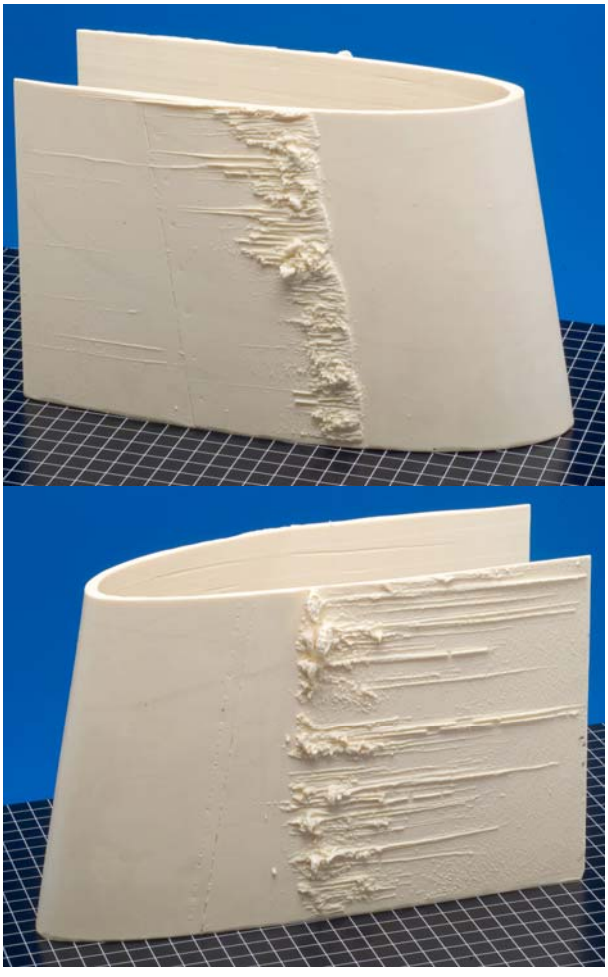

Fig. 3 Photograph of NG0671 runback ice accretion casting, top—upper-surface ridge, bottom—lower-surface ridge.

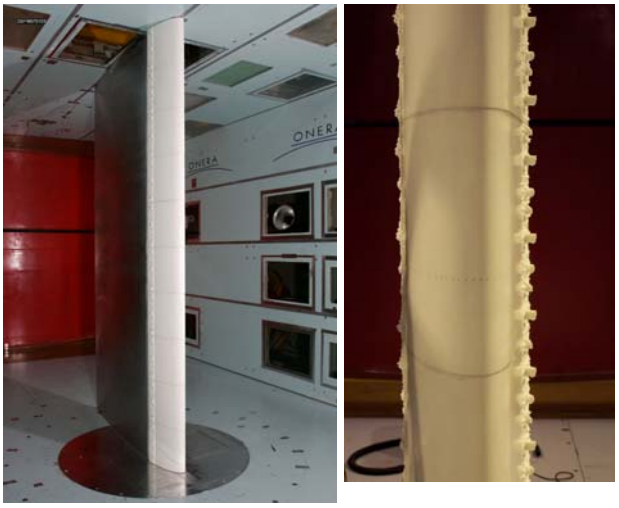

Fig. 4 Completed installation of runback ridge simulation NG0671 on the leading edge of the full-scale NACA 23012 model.

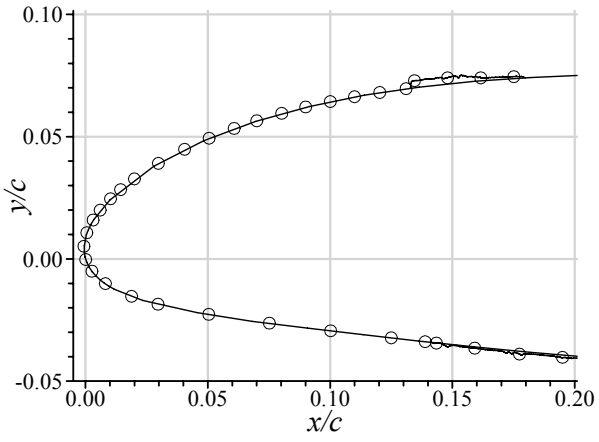

Fig. 5 Tracing of runback ice casting NG0671 on the NACA 23012 leading edge; open circles indicate pressure orifice locations.

D. Subscale Model Ice-Shape Simulation Methods

The subscale NACA 23012 model was tested with several variations of NG0671 runback-ridge simulations. These artificial ice shapes were constructed using commercial, off-the-shelf materials because the runback accretion was too small (upper surface) and too three-dimensional (lower surface) to model with rapid-prototyping methods such as stereolithography. A "build-up" approach was employed whereby individual ice features were added to the upper and lower surface incrementally. This approach yielded an understanding of the aerodynamic effects of individual simulation features. The simulation methods and terminology follow those established in closely related research.[1,12,18,24,25] Table 4 summarizes the individual features that were combined to simulate the NG0671 runback ridge ice accretion. The "SG" notation refers to "simple geometry" which, in this case, means that the runback ridge was simulated with a two-dimensional rectangular shape. This was attached to the model upper surface at x/c = 0.13, identical to the full-scale ice accretion location. The height of the upper-surface ridge was k/c = 0.0028, identical to the maximum height of the upper-surface tracing in Fig. 5. This simulation is designated "SG-US" in Table 4 and was a geometric scaling of the traced cross-section. The actual ice accretion did have some variation in height along the span that was not modeled with the simple-geometry simulation. Following the "build-up" approach, carborundum roughness elements with height k/c = 0.0008 were applied to the top of the simple-geometry ridge ("SG+R-US" in Table 4) to model roughness and height variations in the actual accretion. Instead of roughness, simulated frozen rivulets were applied to the upper surface ridge in a third simulation ("SG+Riv-US). Analogous simple-geometry simulations were also developed and tested on the model lower surface. In this case, using a two-dimensional simulation was difficult to define owing to the highly three-dimensional nature of the lower-surface ice accretion, thus requiring some engineering judgment. The height k/c = 0.0039 selected for the lower-surface SG ridge was based upon matching the combined frontal area of large isolated ice elements. The sensitivity of the lower-surface ice accretion simulation was determined by developing a higher-fidelity, three-dimensional simulation ("3D-LS"). The individual isolated ice elements were geometrically scaled and attached to a thin substrate on the lower surface. In addition, simulated frozen rivulets were also modeled ("3D+Riv-LS") and more documentation is provided in Broeren et al.[23] Aerodynamic testing was performed with various combinations of upper and lower-surface simulations to quantify their effects.

Table 4 Summary of Runback Ridge Ice Simulations.

Simulation	Description
SG-US	Rectangular ridge on upper surface, with height k/c = 0.0028 at x/c = 0.13, chordwise extent $\Delta x/c$ = 0.047
SG+R-US	Roughness elements, height k/c = 0.0008 applied to upper-surface ridge
SG+Riv-US	Simulated frozen rivulets, height k/c = 0.0017 and density of 18 rivulets per inch-span applied to upper-surface ridge
SG-LS	Rectangular ridge on lower surface, with height k/c = 0.0039 at x/c = 0.15, chordwise extent $\Delta x/c$ = 0.042
SG+R-LS	Roughness elements, height k/c = 0.0008 applied to lower-surface ridge
3D-LS	Three-dimensional simulation of lower-surface ridge ice elements, height varied between k/c = 0.0022 and 0.0106
3D+Riv-LS	Simulated frozen rivulets, height k/c = 0.0017 and density of 18 rivulets per inch-span applied to 3D lower-surface ice simulation

III. Results and Discussion

A. Full-scale Results

The effect of the high-fidelity NG0671 runback ice simulation on the performance of the NACA 23012 airfoil is illustrated in Fig. 6 for $Re = 16.0\times10^6$ and M = 0.20. Broeren et al.[22] provide a detailed analysis of the clean NACA 23012 performance data establishing its validity as compared to archival and computational data. For this condition, the maximum lift coefficient of the clean NACA 23012 was 1.82 at an angle of attack of 18.1 deg. The abrupt loss of lift at stall is indicative of leading-edge stall. For this stall type, boundary-layer separation occurs near the leading edge without subsequent reattachment resulting in separated flow over the airfoil and the significant decrease in lift.[26] The pitching-moment coefficient was nearly independent of angle of attack up until about α = 10 deg. The effect of the NG0671 ice simulation was to reduce the lift-curve slope and maximum lift coefficient. The ice simulation produced angle-of-attack dependence of the pitching moment coefficient at much lower angle of attack, commencing at approximately α = 4 deg. The presence of the runback ice simulation resulted in a greater than two-fold increase in drag coefficient over the angle of attack range shown in Fig. 6. The maximum lift coefficient was reduced to 1.51 at α_{stall} = 15.0 deg. in addition to a change in the character of the stall. Analysis of

the surface pressure data and mini-tuft flow visualization indicated significant trailing-edge separation at maximum lift coefficient. However, the decrease in lift for $\alpha > 16$ deg. appeared to be due to flow separation on the entire upper surface originating from the leading edge, or from the spanwise ridge. Therefore, the iced-airfoil stall type was classified as a combination of trailing-edge and leading-edge stall. The evolution of the iced-airfoil stall is discussed in more detail by Broeren et al.[23]

While these are significant performance effects, they are not as severe as for other ice shapes tested on the full-scale NACA 23012 model. Plotted in Fig. 6 for comparison are data for three other ice-casting configurations taken from Broeren et al.[22] Tracings of these ice shapes are shown in Fig. 7. EG1162 and EG1164 were leading-edge ice shapes while EG1159 was a tall spanwise ridge. The performance data show the increasing severity for each configuration in terms of reduced $C_{l,max}$ and α_{stall}, increased pitching-moment slope and increased drag. It is interesting to note that the streamwise ice shape EG1162 resulted in lower drag than the runback ridge NG0671 up to $\alpha \approx 9.5$ deg., as the airfoil with the EG1162 ice shape began to stall. As described in detail by Broeren et al.,[22] the stall of this configuration maintained the character of the abrupt, leading-edge stall type of the clean airfoil. For the EG1164 and EG1159 configurations, the aerodynamics were governed primarily by a large upper-surface separation bubble resulting from the ice accretion. The separation bubble grew larger with increasing angle of attack precipitating the stall at much lower angle of

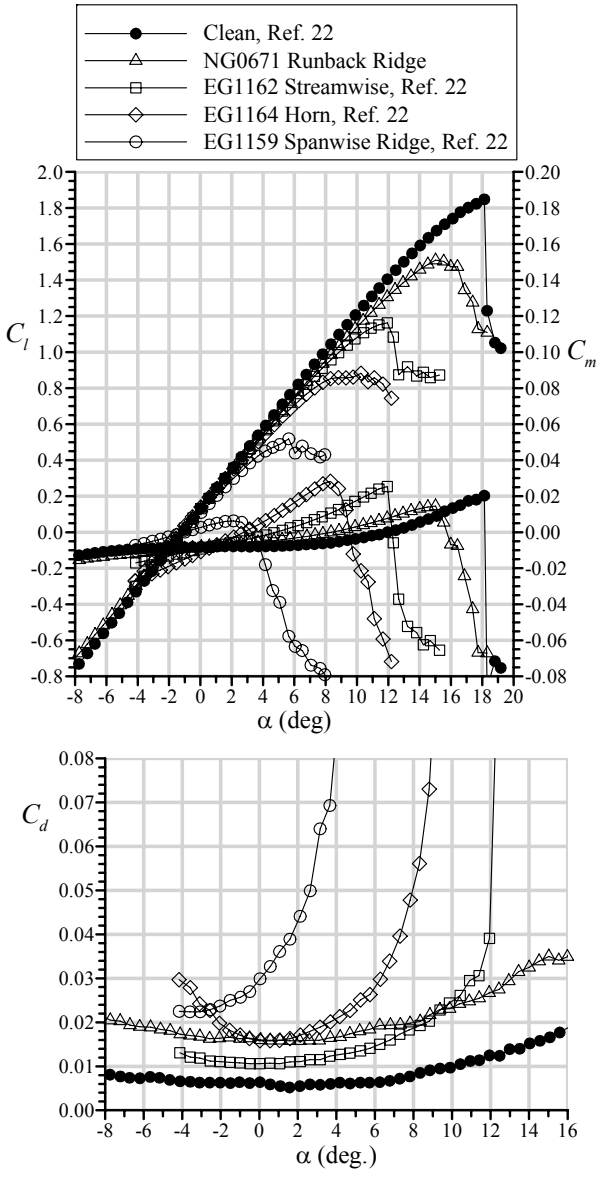

Fig. 6 Comparison of clean and iced NACA 23012 airfoil performance for various high-fidelity ice casting simulations at $Re = 16.0\times10^6$ and $M = 0.20$.

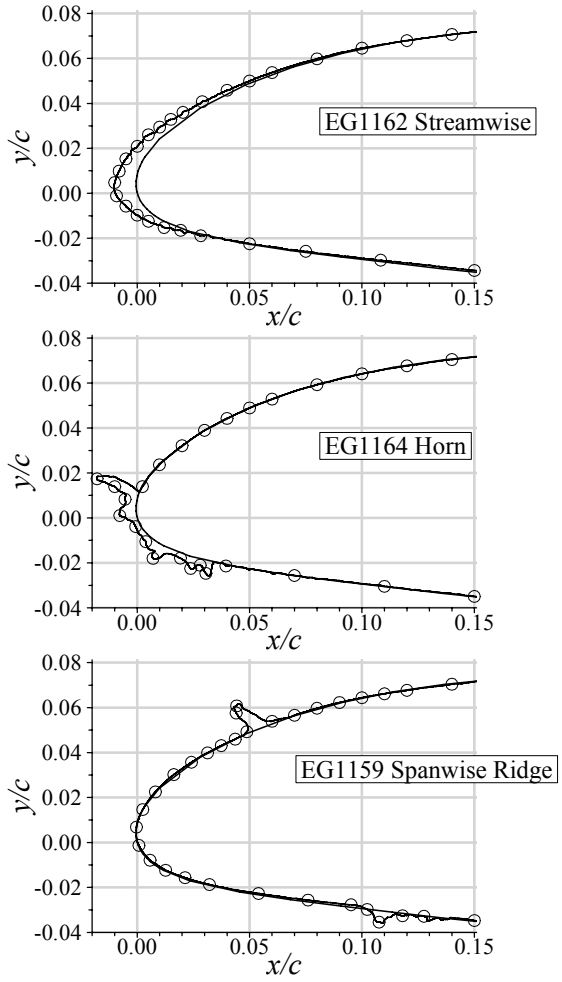

Fig. 7 Tracings of various ice casting simulations tested by Broeren et al.[22] on the full-scale NACA 23012 airfoil model; open circles indicate pressure orifice locations.

attack than for the clean airfoil. This combined with the physical size of the ice shape also contributed to the large increase in drag from the clean airfoil configuration.

The aerodynamic effect of these ice shapes is compared further in terms of surface pressure distribution in Fig. 8. Here the data are split into two separate plots for clarity. First, consider the comparison of the NG0671 runback ridge, EG1162 streamwise ice and clean airfoil configurations. At this angle of attack, there was very little difference in surface pressure between the clean airfoil and the EG1162 configuration. The streamwise ice shape, being conformal to the NACA 23012 leading edge, does not result in large-scale boundary-layer separation or other significant redistribution of static pressure for this angle of attack. This explains, in part, the minimal increase in drag from the clean configuration relative to the other iced configurations for this angle of attack. The surface pressure distribution of the NG0671 configuration clearly reveals the effect of the ice shape on both the upper and lower surface. At this positive angle of attack, the effect on the upper surface was much more pronounced. There was a large change in pressure, from C_p = -0.4 to -2.7 at the forward face of the ridge. These measurements capture the flow deceleration immediately forward of the ridge followed by the flow acceleration over the top of the ridge. This was then followed by a rapid pressure recovery with the static pressure re-conforming to the clean airfoil values at x/c > 0.18. Surface-oil flow visualization revealed the presence of a small separation bubble immediately aft of the ridge with subsequent reattachment within only a few percent chord. An important characteristic here is that the pressure distribution was only altered from the clean configuration in the immediate vicinity of the runback ridge. Furthermore, the effect on the surface pressure was somewhat "symmetric" in that the effect on the integrated lift and pitching moment was small. The effect on pitching moment was also mitigated by the location of the ridge being close to the moment center at x/c = 0.25. Clearly the drag coefficient was increased by the forward face of the ridge and resulting separation. This explains in part why the drag coefficient was higher than for the EG1162 configuration. There was also additional drag due to the ice elements on the lower surface of the NG0671 runback-ridge configuration.

Also plotted in Fig. 8 are surface pressure distributions for the EG1164 and EG1159 iced-airfoil configurations. For these cases, there was a large deviation from the clean airfoil owing to the large extent of separated flow. For the EG1164 shape, the flow separated near the tip of the horn resulting in the region of nearly constant pressure from x/c = -0.02 to 0.03 on the upper surface. There was significant pressure recovery downstream of x/c = 0.03, but C_p did not approach that of the clean airfoil until x/c = 0.20. For the EG1159 spanwise-ridge shape, the separated flow region was much larger as indicated by the region of nearly constant pressure from x/c = 0.04 to 0.30 on the upper surface. This region was followed by a very gradual pressure recovery. Surface-oil flow visualization performed at this angle of attack indicated a time-averaged separation bubble reattachment zone from x/c = 0.64 to 0.68. The pressure data for this case also reveal the large effect of the lower-surface ridge that also had a small separation bubble associated with it. The large extent of separated flow for the EG1159 configuration is consistent with the large degradation in the performance coefficients in Fig. 6.

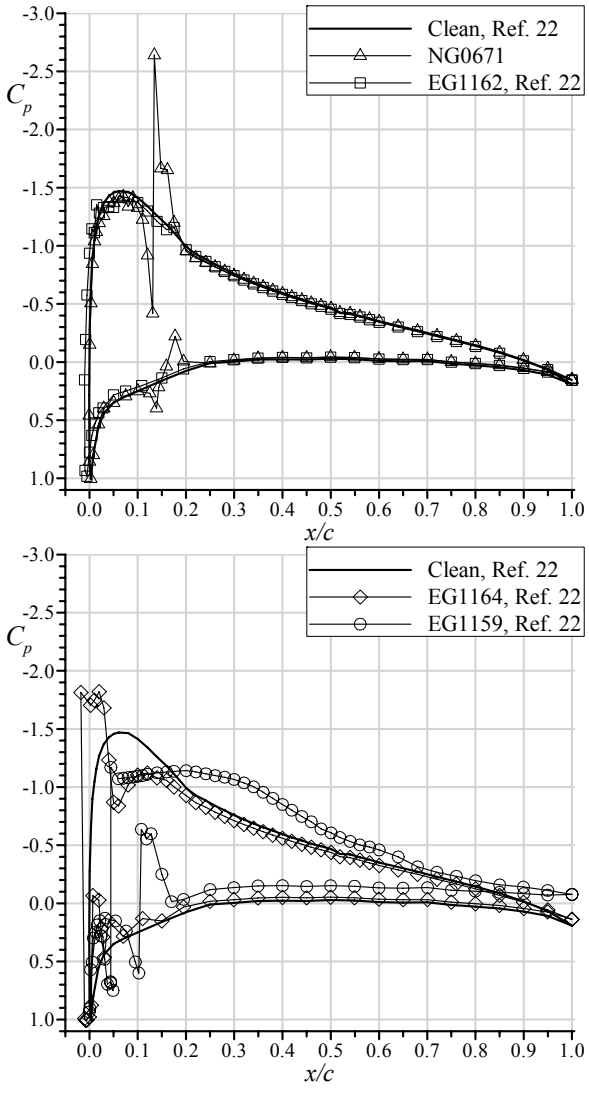

Fig. 8 Comparison of clean and iced NACA 23012 airfoil pressure distribution for various high-fidelity ice casting simulations at α = 4.2 deg., *Re* = 16.0×10^6 and *M* = 0.20.

The pressurization capability of the ONERA F1 wind tunnel was fully exploited to establish the effects of Reynolds and Mach number on the performance of the NACA 23012 airfoil with the NG0671 runback ridge. In general, changes in Reynolds number from 4.7×10^6 to 12.2×10^6 at $M = 0.10$ and from 8.9×10^6 to 16.0×10^6 at $M = 0.20$ had very little effect on the iced airfoil performance as shown in Broeren et al.[23] Changes in Mach number from 0.10 to 0.28 at $Re = 12.2\times10^6$ did have slightly more effect on the iced-airfoil performance, with a small increase in drag coefficient over this range. These results are consistent with previous aerodynamic studies of iced airfoils.[8,22,27-30]

The effect of Reynolds and Mach number on iced-airfoil performance can be further summarized through analysis of the maximum lift coefficient. This parameter is plotted for various configurations against Reynolds number in Fig. 9. These data, along with the data from Broeren et al.,[22] were all acquired in the ONERA F1 wind tunnel. The data from Broeren et al.[8] were acquired in the NASA Langley Low-Turbulence Pressure Tunnel (LTPT). Since both facilities were pressurized wind tunnels, the Mach number was held constant at the values specified. The comparison in $C_{l,max}$ for the clean NACA 23012 airfoil is considered to be good given the potential differences in models, model scale, installation, facilities, as well as experimental uncertainty. The $C_{l,max}$ increased from 1.50 at $Re = 2.0\times10^6$, $M = 0.12$ to 1.88 at $Re = 12.3\times10^6$, $M = 0.10$. As shown in Fig. 9, there was much less Reynolds number dependence of $C_{l,max}$ for the iced-airfoil configurations. There was some variation in $C_{l,max}$ with Reynolds number for the NG0671 runback ridge, but no clear trend. More data are needed to establish what Reynolds number dependence there may be, particularly for $Re < 4.7\times10^6$. Included for comparison to the NG0671 runback ridge are the four ice shapes from Figs. 6-8 and a forward-facing quarter-round spanwise-ridge ice shape. The quarter-round shape had height $k/c = 0.0139$ and was tested at two chordwise locations on the airfoil ($x/c = 0.02$ and 0.10). The data for the leading-edge ice shapes EG1162 and EG1164 show virtually no change in $C_{l,max}$ over the Reynolds number range tested. The data for the EG1159 configuration indicate a small decrease in $C_{l,max}$ for $Re = 4.6\times10^6$ to 12.2×10^6 at $M = 0.10$. The quarter-round cases show even less variation with no significant change in $C_{l,max}$ versus Re from 2.0×10^6 to 10.5×10^6 for these tall spanwise-ridge shapes. The data in Fig. 9 show that Mach number is an equally, if not more, significant parameter for spanwise-ridge ice shapes.

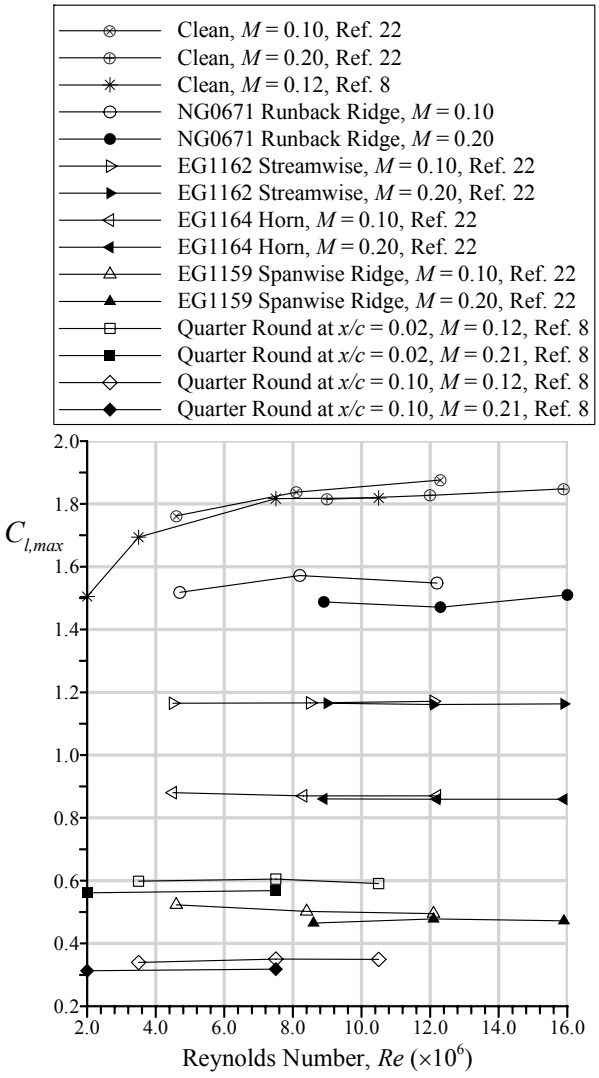

Fig. 9 Effect of Reynolds number on maximum lift coefficient for the NACA 23012 airfoil for clean and iced configurations.

The effect of Mach number on maximum lift coefficient is summarized in Fig. 10 for the same iced-airfoil configurations. The data show good agreement for the values of $C_{l,max}$ on the clean airfoil, particularly for $M > 0.20$. Of the iced-airfoil configurations, the spanwise ridges had the most dependence on Mach number. For the NG0671 runback ridge, the Mach number dependence was similar to, if not more than, the clean airfoil. The $C_{l,max}$ for the airfoil with the tall spanwise-ridge shapes (EG1159 and quarter round) also shows some Mach number dependence. Iced-airfoil Mach number effects have been addressed in other studies.[2,31]

Aside from the Reynolds and Mach number effects, a more significant effect for the tall ridge shapes is the upper-surface location of the ridges. Close inspection of Fig. 7 yields a ridge height, $k/c = 0.013$ at $x/c = 0.05$ in chordwise location. This is very similar in height to the $k/c = 0.0139$ quarter-round

shape data in Figs. 9 and 10. Lee and Bragg[7] researched the impact of ridge location and airfoil type on aerodynamic performance degradation. They found that $C_{l,max}$ was a strong function of spanwise-ridge location between x/c = 0.0 and 0.10 for this airfoil. This explains why there is such a large difference in $C_{l,max}$ between the quarter round at x/c = 0.02 and 0.10 and why the data for the EG1159 ridge fit neatly in between.

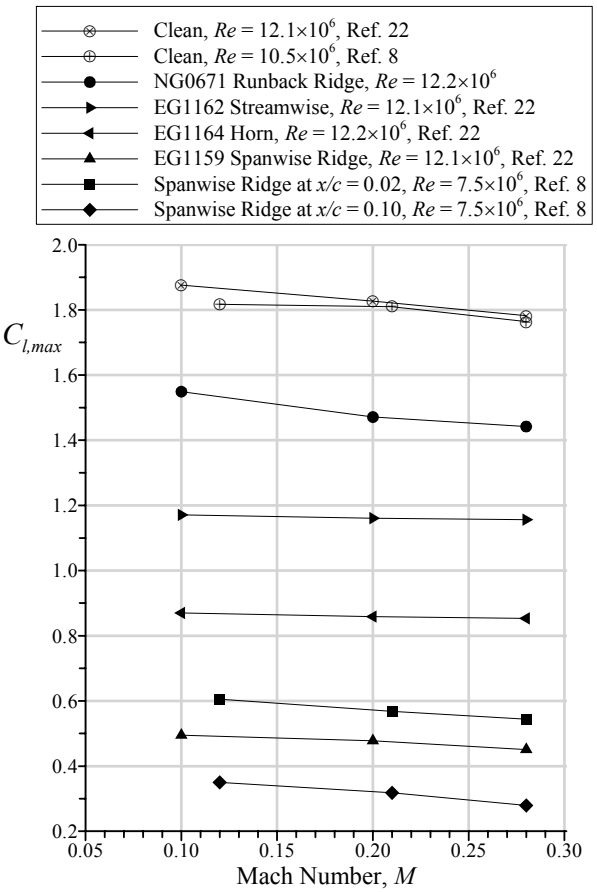

Fig. 10 Effect of Mach number on maximum lift coefficient for the NACA 23012 airfoil for clean and iced configurations.

B. Subscale Simulation of Runback Ridge Aerodynamics

Simulating the aerodynamics of a runback ridge on a quarter-scale model at low-Reynolds number can be challenging because of Reynolds number effects for the *clean* airfoil. This conundrum is illustrated in Fig. 11 which shows that the iced-airfoil configuration at Re = 16.0×10^6 and M = 0.20 had slightly higher lift-curve slope, $C_{l,max}$ and α_{stall} than the clean airfoil at Re = 1.8×10^6 and M = 0.18. The iced-airfoil configuration also had slightly less dependence of C_m on angle of attack. Only the drag coefficient was significantly different from the low-Reynolds number clean configuration. These data may explain the apparent anomalies in previous subscale runback-ridge aerodynamic studies. For example, Calay et al.[4] observed small increases in $C_{l,max}$ and α_{stall} with a k/c = 0.0035 simple-geometry ridge on a NACA 0012 airfoil at Re = 1.25×10^6 and M = 0.08. Similarly, Papadakis and Gile-Laflin[5] also observed lift performance increases for simple-geometry ridges on a NACA 63_A-213 airfoil at Re = 2.0×10^6 and M = 0.17. Whalen et al.[9,10] and Lee et al.[13] are further examples. As shown in Fig. 11, the decrease in maximum lift coefficient and stalling angle of attack for the clean airfoil from Re = 16.0×10^6 to Re = 1.8×10^6 was larger than the degradation due to the NG0671 ice casting simulation at Re = 16.0×10^6. Therefore, subscale simulations of the NG0671 ice shape at low-Reynolds number must result in a slight increase in maximum lift and stalling angle relative to the clean airfoil in order to simulate the iced-airfoil aerodynamics at higher Reynolds number. In the current study, the challenge was to identify the accuracy to which the aerodynamics of the NG0671 runback ridge could be simulated on the quarter-scale model at low-Reynolds number.

The present approach employed simple-geometry ridge simulations in various configurations. The initial performance results are shown in Fig. 12 for three subscale configurations at Re = 1.8×10^6 and M = 0.18 compared to the full-scale NG0671 ice casting and clean configurations at Re = 16.0×10^6 and M = 0.20. The data for the "SG-US" configuration show the effect of the k/c = 0.0028 upper-surface, simple-geometry ridge. The lift-curve slope for this configuration was slightly lower than the airfoil with the NG0671 casting, but the $C_{l,max}$ value of 1.50 and α_{stall} value of 15.4 deg. compared very favorably with the full-scale data. The leading-edge stall characteristics of the clean airfoil persisted in the subscale iced-airfoil case in contrast to the full-scale casting simulation that had characteristics of trailing-edge stall. Despite the good comparison in $C_{l,max}$ and α_{stall}, the character of the iced-airfoil stall was not adequately simulated with the simple-geometry ridge on the upper surface. It is interesting to note, however, that the "SG-US" simulation did slightly increase both $C_{l,max}$ and α_{stall} relative to the clean airfoil values at the same Reynolds and Mach number, consistent with previous reports.[4,5,9,10] Figure 12 also shows that the "SG-US" subscale simulation caused a stronger dependence of the pitching moment coefficient on angle of attack than for the full-scale, iced airfoil. The effect on drag coefficient was larger at higher angle of attack, since the "SG-US" simulation was located on the upper surface. The addition of the lower-surface ridge ("SG-US & SG-LS") improved the drag coefficient comparison while having very little effect on the stalling characteristics. This superposition of iced-airfoil effects has been observed in other studies of horn-type ice shapes[2,32] and spanwise-ridge

shapes.[33] Therefore, it was expected that the addition of the lower-surface ridge would primarily affect the drag, with little or no effect on lift and pitching moment at higher angle of attack.

The effect of added roughness was determined via carborundum grains with $k/c = 0.0008$ applied to each upper and lower-surface simple-geometry ridges. The lift data show that this had a very significant effect on the maximum lift coefficient and stalling angle of attack such that the comparison with the full-scale casting configuration was poor. These results are consistent with the conclusions of Calay et al.[4] and Whalen et al.[9] who noted that the stalling characteristics of the airfoil with simulated runback ridges can be very sensitive to the height and/or geometry of the ridge. As expected, the addition of the roughness on the lower-surface ridge increased the drag coefficient for this configuration at lower angle of attack, thus improving the drag comparison with the full-scale casting. However, the large deviations beginning at approximately 2 deg. were due to the roughness applied to the upper-surface ridge and were consistent with the lower maximum lift coefficient and stalling angle.

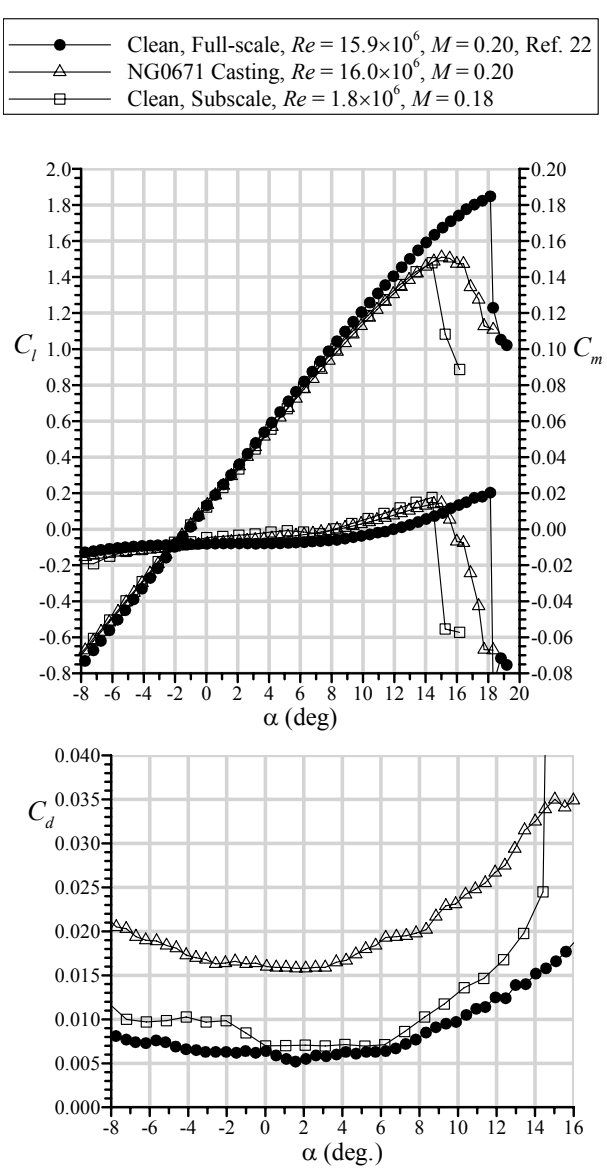

Fig. 11 Comparison of C_l, C_m and C_d vs. α for the clean subscale model and the full-scale NG0671 casting and clean configurations.

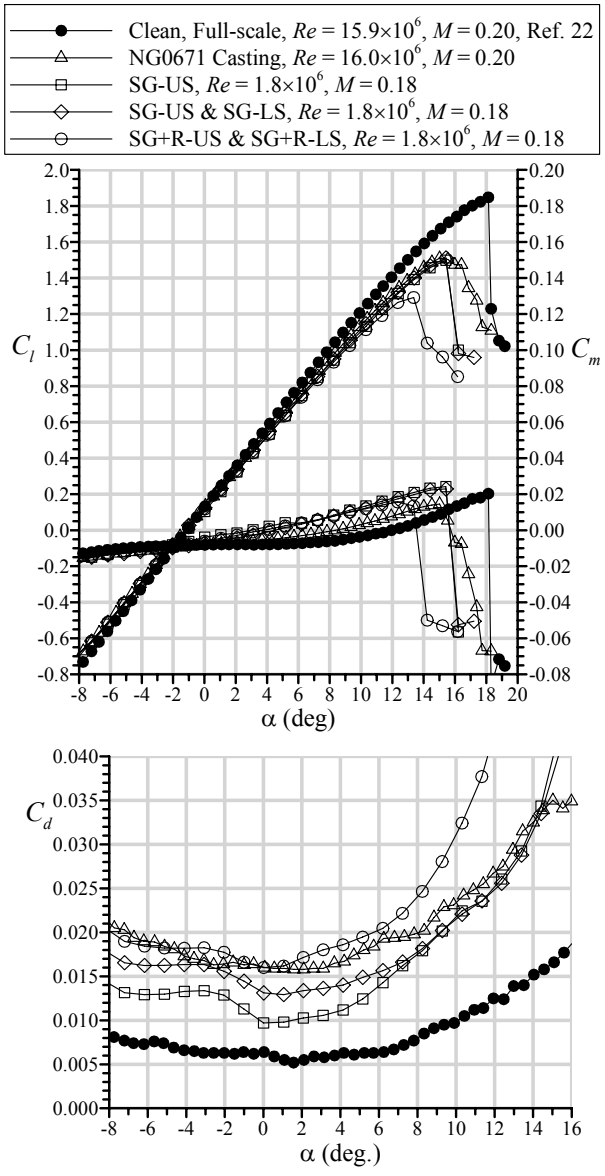

Fig. 12 Comparison of C_l, C_m and C_d vs. α for various subscale runback-ridge simulations and the full-scale NG0671 casting and clean configurations.

The differences in the aerodynamic effect of these simulations is further illustrated in the surface pressure distributions. Figure 13 compares the pressure coefficients for the upper and lower-surface, simple-geometry ridges with and without applied roughness to the full-scale NG0671 casting and clean configurations at a matched angle of attack of 12.4 deg. The three runback-ridge simulations share some similarities. There were not significant differences between the clean and iced pressure distributions, except in the vicinity of the upper-surface ridge. For all of the iced configurations, the presence of the upper-surface ridge caused a small reduction in the magnitude of the suction peak and lower suction pressures downstream on the upper surface relative to the clean airfoil. The pressure coefficients near the trailing edge, particularly for the subscale ice simulations, were also lower, possibility indicating local boundary-layer separation at this angle of attack. The pressure distribution for the full-scale NG0671 casting configuration compared very favorably with the upper and lower surface simple-geometry ridge simulation ("SG-US & SG-LS"). The large suction peak near the forward face of the ridge for the casting configuration was not measured for the subscale simulations since the subscale simulations were not instrumented with pressure taps. The favorable comparison between the pressure distributions for the NG0671 casting and the subscale simple-geometry ridges (without added roughness) further confirms that there is proper simulation of the aerodynamics. The pressure distribution for the simple-geometry ridges with added roughness ("SG+R-US & SG+R-LS") shows a deviation in C_p just downstream of x/c = 0.17 on the upper surface. This deviation likely indicates the presence of a larger separation bubble region downstream of the ridge than for the other two configurations, since it had a noticeable effect on the pressure distribution. This larger separation bubble contributed to the stall at lower angle of attack compared to the no-roughness case as well as the increased drag at higher angle of attack.

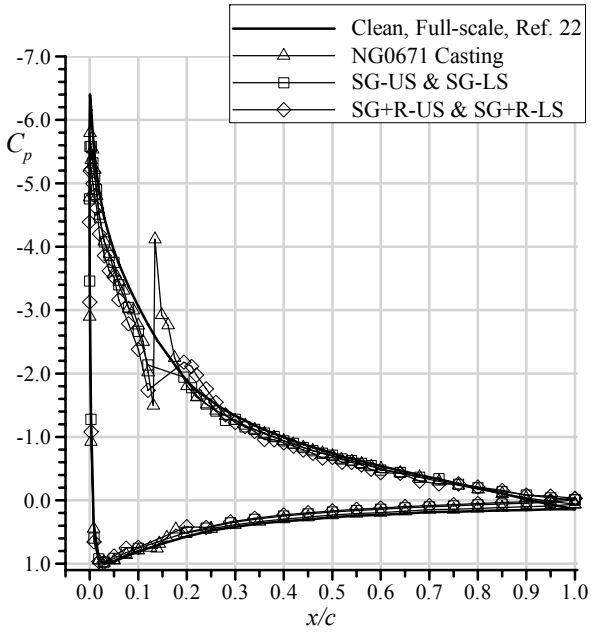

Fig. 13 Comparison of surface pressure distribution for selected subscale runback-ridge simulations (at $Re = 1.8\times10^6$, $M = 0.18$) and the full-scale NG0671 casting and clean configurations (at $Re = 16.0\times10^6$, $M = 0.20$), all at $\alpha = 12.4$ deg.

Drag coefficient comparisons are more difficult to evaluate since there is usually not a single value of importance as is case with maximum lift coefficient. A useful metric for comparing C_d at multiple angles of attack is the percent root-mean-square (RMS) difference in C_d over an appropriate angle of attack range.[12] The angle of attack range used in this study was that over which C_l varied linearly with α. The value $\Delta C_{d,rms}$ is a percentage and is computed by determining the RMS of the percent difference in C_d between the full-scale casting and subscale simulation at each angle of attack in the linear lift-coefficient range (a total of N angles of attack):

$$\Delta C_{d,rms} = \sqrt{\frac{\sum_{i=1}^{N}\left(\frac{C^i_{d,sim} - C^i_{d,casting}}{C^i_{d,casting}}\times 100\%\right)^2}{N}} \qquad (1)$$

While this parameter is useful for making comparisons over an angle of attack range, a disadvantage is that it does not give any indication as to whether or not the C_d of a given subscale simulation is higher or lower than that of the full-scale casting. For this study the selected angle of attack range was -4 deg. to 12 deg. Inspection of Fig. 12 indicates that the "SG-US & SG-LS" subscale simulation had the best overall comparison in C_d to the airfoil with the NG0671 casting. The $\Delta C_{d,rms}$ for this case was 13.0%. The other two subscale simulations had $\Delta C_{d,rms}$ values that were nearly twice as large. For comparison, the $\Delta C_{d,rms}$ for the full-scale NG0671 casting relative to the clean airfoil was 162%, indicating the large overall increase in drag due to the ice shape.

Since the addition of roughness to the upper-surface simple-geometry ridge resulted in a large deviation in C_d relative to the NG0671 casting configuration, data were acquired with roughnesses added to the lower-surface ridge only. These data, labeled "SG-US & SG+R-LS," are shown in Fig. 14. As expected the stalling characteristics were similar to the configuration with only the upper-surface simple-geometry ridge (cf. Fig. 12) while the agreement in drag coefficient was also improved. The $\Delta C_{d,rms}$ value was reduced to 10.2% for this configuration. Attempts at further improving the aerodynamic simulation were not successful. A three-dimensional lower-surface simulation was fabricated that closely modeled the individual ice elements of the NG0671 ice shape. This was tested along with the simple-geometry ridge on the upper surface ("SG-US & 3D-LS" in Fig. 14). As expected, the influence of this change was primarily observed in the drag coefficient for $\alpha < 4$ deg. The corresponding values of C_d were significantly higher than for the airfoil with the NG0671 casting. This led to a $\Delta C_{d,rms}$ value of 14.3%. Finally, simulated frozen rivulets were applied to the upper-surface simple-geometry ridge and to the lower-surface 3D simulation ("SG+Riv-US & 3D+Riv-LS" in Fig. 14). This simulation was tested because it was thought to best represent the highest-fidelity subscale simulation possible using commercial, off-the-shelf materials. Such a simulation may be considered "the most representative" without *a priori* knowledge of the full-scale, iced-airfoil aerodynamics. As shown in Fig. 14, the effect on performance was very similar to the addition of roughness to the simple-geometry ridges. The simulated frozen rivulets on the upper surface caused a reduction in maximum lift coefficient and stalling angle. The drag at angles of attack larger than 2 deg. was significantly increased. These results are consistent with Whalen et al.[9] who noted that three-dimensional runback ridge simulations tended to yield larger performance penalties than their two-dimensional counterparts.

The subscale simulation effectiveness is summarized for each configuration in Table 5 where $C_{l,max}$, α_{stall} and $\Delta C_{d,rms}$ were computed relative to the full-scale NG0671 casting configuration. According to these parameters, the best simulation was the simple-geometry ridge on the upper and lower surface with roughness applied to the lower-surface ridge only ("SG-US & SG+R-LS"). This adequately simulated the full-scale iced-airfoil aerodynamics, with the exception of the stall type. This simulation on the subscale model stalled from the leading edge, in contrast to the full-scale iced-airfoil that had a more gradual trailing-edge stall. However, none of the subscale simulations tested were able to reproduce the stall characteristics of the full-scale iced airfoil. In addition, the pitching-moment coefficient also exhibited greater angle of attack dependence for all of the subscale simulation configurations relative to the full-scale iced airfoil. As previously discussed, the addition of roughness to the upper-surface simple-geometry ridge resulted in larger performance degradations. Similar results, though less severe, were obtained when simulated frozen rivulets were applied to the upper-surface simple-geometry ridge. Variations in the lower-surface ridge simulations primarily affected drag coefficient, predominately at lower angle of attack.

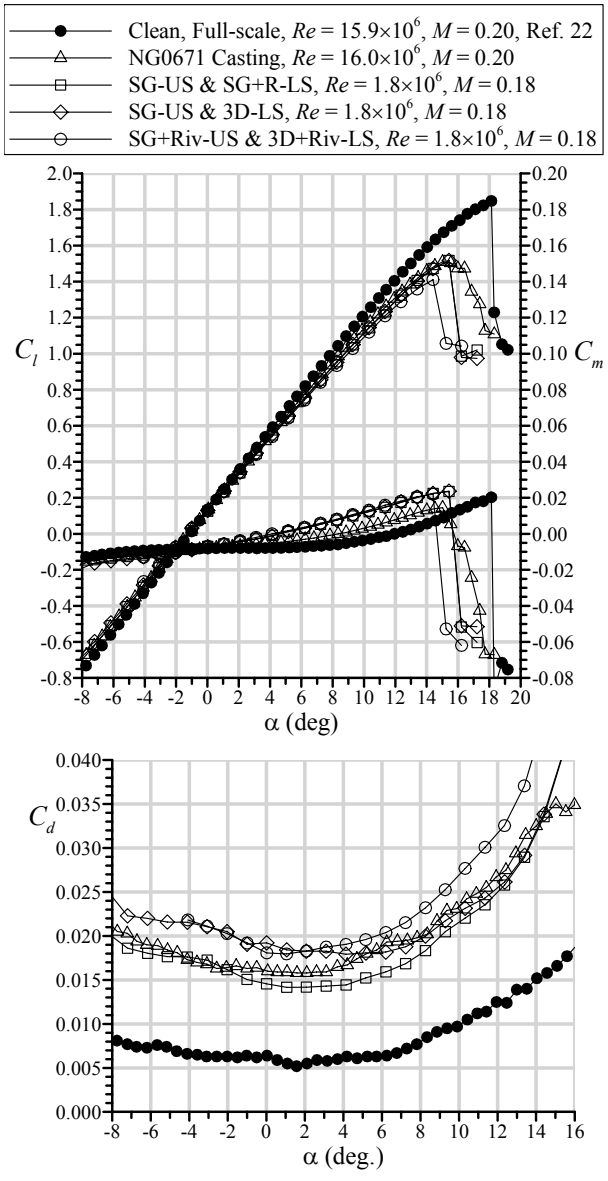

Fig. 14 Comparison of C_l, C_m and C_d vs. α for various subscale runback-ridge simulations and the full-scale NG0671 casting and clean configurations.

Table 5 Summary of Subscale Model Simulation Effectiveness for the NG0671 Ice Casting.

Simulation	Sim. $C_{l,max}$ - Casting $C_{l,max}$	Sim. α_{stall} - Casting α_{stall} (deg.)	Sim. vs. Casting $\Delta C_{d,rms}$
SG-US	-0.01	0.4	25.6%
SG-US & SG-LS	0.00	0.4	13.0%
SG+R-US & SG+R-LS	-0.22	-1.6	23.8%
SG-US & SG+R-LS	0.01	0.4	10.2%
SG-US & 3D-LS	0.01	0.4	14.3%
SG+Riv-US & SG+Riv-LS	-0.10	-0.6	16.7%

These data support the findings of previous researchers in regard to the aerodynamic effects of short, spanwise-ridge ice shapes. The geometric details of the subscale simulation, such as surface roughness, can have a significant effect on the iced-airfoil aerodynamics. Design and fabrication of three-dimensional subscale simulations and/or adding roughness are consistent with common practices. The present results indicate that such simulations tested at low-Reynolds number will likely result in conservative performance degradations. It was also observed that the two-dimensional, simple-geometry simulations on the upper surface (without added roughness) on the subscale model yielded slight increases in maximum lift coefficient and stalling angle compared to the clean configuration at $Re = 1.8\times10^6$. As reported by Whalen,[9,33] these short ridge simulations sometimes act to delay boundary-layer separation, causing an increase in airfoil performance near stall. This gives rise to an apparently anomaly where the iced-airfoil stall performane was improved from the clean configuration at $Re = 1.8\times10^6$. Since the iced-airfoil results show good agreement with the full-scale iced-airfoil results, this apparent anomaly exists because of the reduction in clean airfoil lift performance with Reynolds number. What is unknown is the effect of Reynolds number between 1.8×10^6 and 4.7×10^6 for the artificial ice shapes tested on the subscale model or, alternatively, for the high-fidelity simulation tested on the full-scale model. That is, an exact scale model of the NG0671 casting was not tested on the subscale model; nor was an exact scale model of the simple-geometry ridges tested on the full-scale model. This represents a Reynolds number gap between $Re = 1.8\times10^6$ and 4.7×10^6, and a knowledge gap in our understanding of runback-ridge aerodynamics. The present data show that a simple, two-dimensional, geometrically scaled ridge simulation best represents the full-scale, high-Reynolds number, iced-airfoil aerodynamics on a subscale model at $Re = 1.8\times10^6$.

Whalen et al.[9,10,21,33] investigated boundary-layer based scaling methods for runback ice accretion. Depending upon the airfoil angle of attack and chordwise location of the ice accretion, the boundary-layer thickness was found to be similar to the ice accretion height in some cases. This led to a method of sizing the artificial ice shapes based on the ratio of the boundary-layer thickness between the full-scale and subscale models at their respective Reynolds numbers. The boundary-layer scaled ice shapes were nearly a factor of two larger than the geometrically scaled ice shapes since boundary-layer thickness increases as Reynolds number decreases. In that study, the larger, boundary-layer scaled ice shapes resulted in larger aerodynamic penalties than did the geometrically scaled ice shapes. Since full-scale aerodynamic data were unavailable for validation, it was unclear as to which scaling method was appropriate. Based upon the present data, it appears that the larger boundary-layer scaled simulations resulted in unrealistically large performance penalties relative to an equivalent full-scale, high-Reynolds number configuration.

Simulation methods for Reynolds numbers lower than 1.8×10^6, may require other alternatives to geometric and boundary-layer scaling. Figure 15 shows the change in performance for the best simple-geometry simulation of the NG0671 casting with Reynolds and Mach number decreased to 1.0×10^6 and 0.10, respectively. For the lower Reynolds number, the lift-curve slope approaching stall is reduced along with the maximum lift coefficient and stalling angle of attack. Interestingly, the pitching-moment and drag coefficients are largely unaffected by the decrease in Reynolds and Mach number. These data imply that an artificial ice shape smaller than the geometry-based scaling is required to adequately simulate the full-scale aerodynamics. In fact this was the case for Lee et al.[13] in their investigation of geometry and Reynolds number scaling of runback ice accretion on a business jet wing. In that study, 5/12-scale and 1/12-scale models were used to simulate the runback ice accretion effects on a full-scale wing panel at $Re = 4.2\times10^6$. The authors found that artificial ice shapes smaller than geometrically scaled simulations were required to reproduce equivalent aerodynamic effects on the smaller scale models. Reynolds numbers as low as 0.15×10^6 were used for the 1/12-scale model. However, Lee et al. were not fully successful in simulating the full-scale model aerodynamics with the 1/12-scale model for runback ice accretion. This was

attributed to the large difference in model scale (factor of 12) and Reynolds number (factor of 28). In many cases the clean-wing performance of the 1/12-scale model was degraded more than the iced-wing performance of the full-scale model.

C. Aerodynamic Classification of Spanwise-Ridge Ice

The data in Fig. 6 illustrate the contrasting aerodynamic effects between short spanwise ridges as exemplified by the NG0671 shape and tall spanwise ridges as exemplified by the EG1159 shape. Clearly, the aerodynamics are fundamentally different. The ice-accretion classification developed by Bragg et al.[2] for spanwise ridges was primarily based upon research related to tall ridges similar to the EG1159 shape. In this paper a subclassification is proposed that divides spanwise-ridge ice into "short" and "tall" ridges. The definition of these terms is not to be taken in regard to the physical height, but rather the associated effect on the flowfield and pressure distribution. Specifically, the distinction between short and tall ridges lies in consideration of the separation bubble generated by the presence of the spanwise ridge and the resulting aerodynamics.

The subclassification is analogous to the separation bubble nomenclature proposed by Tani.[34] In his review of airfoil separation bubble characteristics, Tani defined the terms "short" and "long" not based upon length, but based upon the effect on pressure distribution. He wrote, "The presence of a long bubble makes the pressure distribution radically different from that in inviscid flow, with the result that the sharp suction peak near the leading edge is not realized. Instead, a suction plateau of a reduced level extends over the region occupied by the bubble length." In contrast, a short bubble has a minimal effect on the pressure distribution and leading-edge suction peak. The distinction between short spanwise-ridge ice and tall spanwise-ridge ice can be made in terms of the resulting separation bubble and its effect on the flowfield as manifest in the pressure distribution.

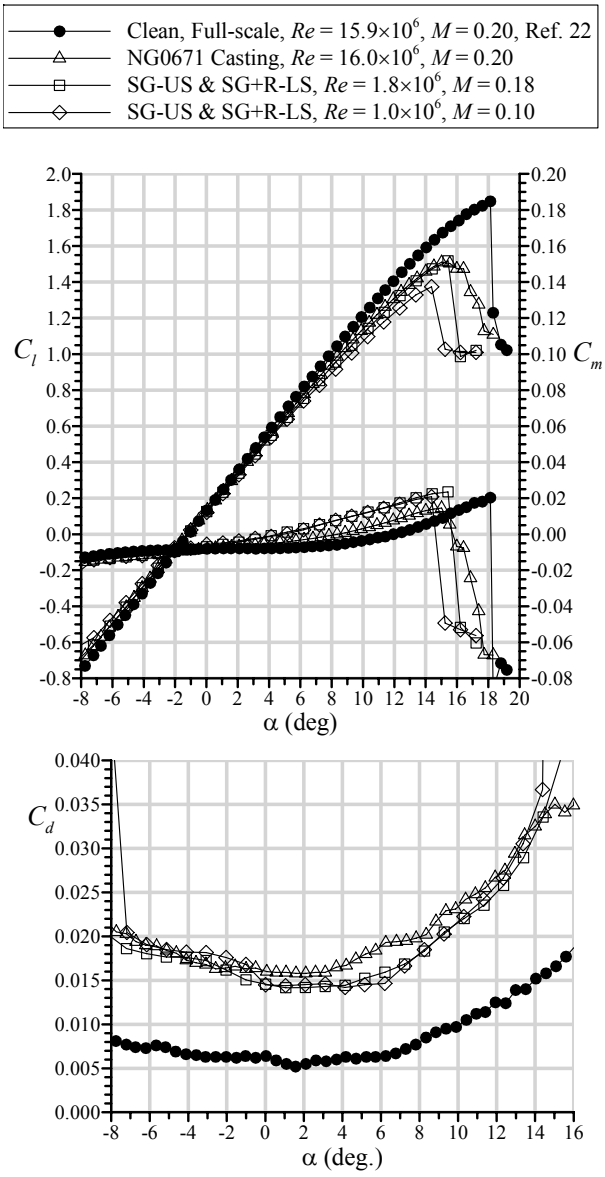

Fig. 15 Effect of Reynolds and Mach number on the subscale runback-ridge simulation aerodynamic performance.

Numerous investigations into the aerodynamics of tall spanwise ridge ice shapes have been conducted[6-8,35-37] and the results are very briefly summarized here. As previously mentioned the salient feature of the tall spanwise-ridge flowfield is the separation bubble that forms downstream of the ice shape. The resulting re-distribution of surface pressure is significant as illustrated in Fig. 8 for the EG1159 ice shape. The iced-airfoil pressure distribution bears almost no similarity to the clean airfoil pressure distribution at the same angle of attack. Lee and Bragg[6] documented the growth of the upper-surface separation bubble with angle of attack for the tall, forward-facing, quarter-round, spanwise-ridge shape using surface-oil flow visualization. The k/c = 0.0139 ice shape was located at x/c = 0.10 on the upper surface of the NACA 23012m airfoil and tested at $Re = 1.8\times10^6$ and M = 0.18. The bubble reattachment region was centered at about x/c = 0.42 at α = 0 deg. The bubble grew rapidly with increasing angle of attack, until the reattachment region reached the trailing edge at about α = 4 deg., precipitating the stall with maximum lift coefficient of about 0.25. As discussed at length by Bragg et al.,[2] these large separation bubbles are known to have large-scale unsteady characteristics. Since the surface-oil flow visualization technique is essentially a time-averaged method, only the region of mean reattachment was indicated. Also investigated were the effect of ridge height, cross-sectional

geometry, location and airfoil geometry. The height of the spanwise ridge was found to have a strong influence on the iced-airfoil aerodynamics as well as the chordwise location of the ridge for certain airfoils. Cross-sectional geometry was also found to be an important factor. As discussed in connection with Fig. 9, there were negligible Reynolds number effects on maximum lift coefficient at constant Mach number down to $Re = 2.0\times10^6$. Lee and Bragg[6,7] showed continued Reynolds number independence down to $Re = 1.0\times10^6$ and $M = 0.10$ for the $k/c = 0.0139$ quarter-round shape located at $x/c = 0.10$. So it can be seen that tall spanwise-ridge shapes have a large effect on the airfoil pressure distribution in terms of deviation from the clean configuration. This is manifested through a large separation bubble that grows in size (in the time-averaged sense) with small increases in angle of attack. Finally, the effect of Reynolds number on the flowfield and performance has been shown to be negligible for the iced airfoil down to $Re = 1.0\times10^6$.

Short spanwise ridges exemplified by the NG0671 ice shape have different characteristics. As discussed in connection with Fig. 8, the effect of the simulated runback ridge on the pressure distribution was only a localized disturbance in the immediate vicinity of the ridge (both upper and lower surface for the NG0671 configuration); elsewhere the surface pressure closely matched that of the clean airfoil. Like Tani's short and long bubbles, this distinction—effect on pressure distribution—determines what is a short or tall spanwise ridge shape. The question then remains to determine how obvious this distinction may be for shapes of intermediate heights. Whalen[33] performed an extensive parametric study of 2-D square-cylinder simple-geometry simulations of spanwise ridges on a NACA 3415 airfoil at $Re = 1.8\times10^6$ and $M = 0.18$. The effect on pressure distribution for increasing ice-shape height for two different angles of attack is shown in Fig. 16. This airfoil model was equipped with a plain flap with hinge located at $x/c = 0.75$. The flap was not deflected for these experiments and the lower-surface gap was sealed. The data for $\alpha = 10$ deg. show the increasing aerodynamic effect of the square-ridge shapes for increasing height. The large discontinuity in C_p is observed at the ice-shape location of $x/c = 0.16$ on the upper surface. Clearly, the pressure distribution for the smallest shape ($k/c = 0.0035$) had features analogous to that of the NG0671 runback ridge. In the former case, the presence of the simple-geometry ridge caused a slight decrease in the suction pressure from the leading-edge peak downstream to the ice shape (at $x/c = 0.16$) relative to the clean configuration. Increasing the angle of attack to 13 deg. shows much better alignment with the clean surface pressures except in the immediate vicinity of the ridge.

This behavior is contrasted with the $k/c = 0.0069$ shape. Even at the lower angle of attack of 10 deg., the effect of this simulated ice shape on the surface pressure was profound. It exhibited the classic characteristics of tall spanwise ridges. The pressure distribution for the iced airfoil had significant deviation from the clean airfoil configuration. The pressure plateau from $x/c = 0.17$ to 0.24 and subsequent gradual pressure recovery are indicative of a large separation bubble. This was confirmed via surface-oil flow visualization that indicated a time-averaged reattachment location at $x/c = 0.45$. The deviation of surface pressure from the clean configuration downstream of $x/c = 0.65$ on the upper surface was indicative of boundary-layer separation that was also

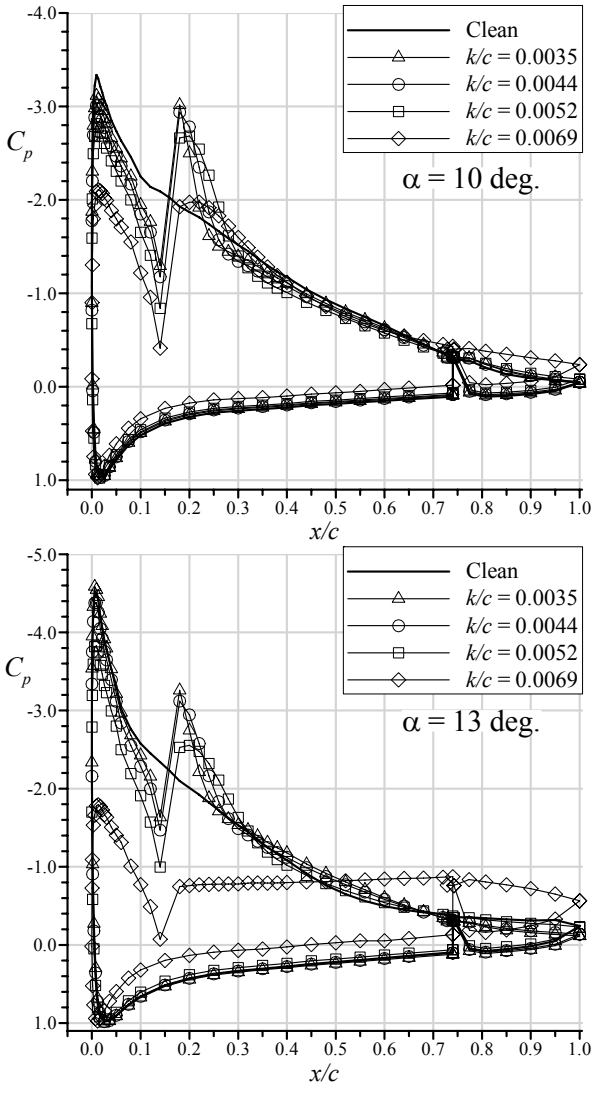

Fig. 16 Surface pressure effect of square-cylinder spanwise-ridge height at $x/c = 0.16$ on the upper surface of the NACA 3415 airfoil at $Re = 1.8\times10^6$, $M = 0.18$, adapted from Whalen.[33]

confirmed in the flow visualization. The increase in angle of attack to 13 deg. for this configuration indicates a stalled flow condition. Based upon these observations, the distinction between the k/c = 0.0035 and 0.0069 shapes is clear.

For the intermediate height simple-geometry ridges, the distinction between what would be considered tall or short may not be as obvious. However, further comparison of the pressure distributions in Fig. 16 reveals some important characteristics. For α = 10 deg., there are only minor differences in the pressure distributions for the k/c = 0.0044 and 0.0052 configurations. The biggest difference is that the airfoil with the k/c = 0.0044 shape attained a lower pressure just downstream of the ridge (x/c = 0.018), having nearly the same value as for the k/c = 0.0035 shape ($C_p \approx$ -2.9). The k/c = 0.0044 shape also resulted in a steeper pressure recovery while the k/c = 0.0052 configuration exhibited a short pressure plateau region with more gradual pressure recovery. The latter is indicative of a large separation bubble. Therefore, based on the proposed definition, the k/c = 0.0044 ridge would be considered a short spanwise ridge, while the k/c = 0.0052 would be considered a tall spanwise ridge. This is confirmed in the pressure data for α = 13 deg. Here, the pressure distribution for the k/c = 0.0044 configuration conformed to the clean airfoil C_p, except in the immediate vicinity of the ridge, while the pressure distribution for the k/c = 0.0052 configuration more clearly indicates the presence of a large separation bubble. Therefore, for the case of a spanwise-ridge ice shape located at x/c = 0.16 on the upper surface of the NACA 3415 airfoil at Re = 1.8×10^6 and M = 0.18, the boundary between what is a short spanwise ridge and tall spanwise ridge lies somewhere between k/c = 0.0044 and 0.0056. Of course, this distinction is somewhat arbitrary. In reality, there is clearly an overlap region in the proposed subclassification as there is in any continuum.

Whalen et al.[9,10,21,33] further investigated the flowfield for the k/c = 0.0035 and 0.0069 spanwise ridges using surface-oil flow visualizations and hot-wire boundary-layer measurements. Consistent with previous findings for tall spanwise ridges was the presence of a large separation bubble that grew rapidly with angle of attack for the k/c = 0.0069 ridge. The flowfield for the airfoil with the k/c = 0.0035 spanwise ridge was fundamentally different. Although there was a small separation bubble, the reattachment location was nearly constant over a large angle of attack range. Figure 17 is a plot of the bubble reattachment location versus angle of attack for three different configurations. Included with the square-cylinder shapes on the NACA 3415 airfoil are data from Lee and Bragg[6] for the k/c = 0.0139 quarter-round shape on the NACA 23012m airfoil. The data clearly illustrate the difference in angle of attack dependence of the separation bubble reattachment location. The error bars illustrate the size of the reattachment region due to the aforementioned unsteady characteristics associated with these large separation bubbles. In contrast to the tall shapes, the error bars for the short, k/c = 0.0035 shape on the NACA 3415 airfoil illustrate the more steady character of the bubble. For the tall-ridge configurations, the stall was driven by the increasing size of the separation bubble. But in the case of the short-ridge configuration, the principal stall mechanism was from trailing-edge separation moving forward with increasing angle of attack.

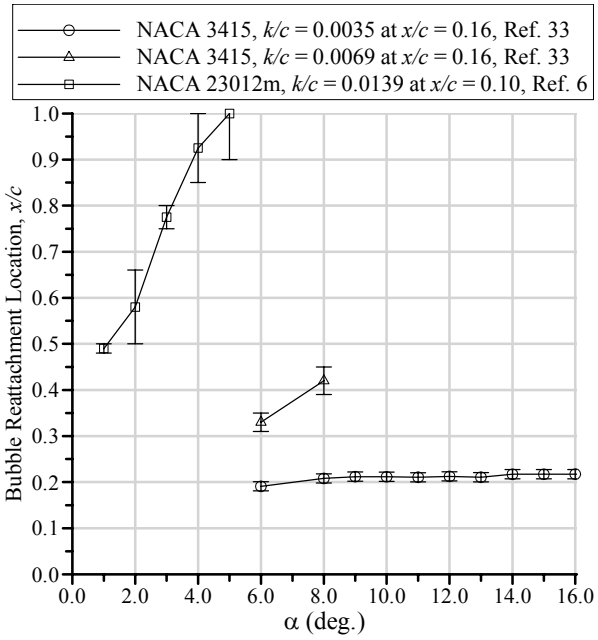

Fig. 17 Comparison of separation bubble reattachment location based on surface oil flow visualization results for tall and short spanwise ridges, all data at $Re = 1.8\times10^6$, $M = 0.18$.

The differences in the separation bubble details are also illustrated in the single-component hot-wire mean and RMS velocity profiles in Figs. 18 and 19. The profiles were measured on the NACA 3415 airfoil upper surface for the k/c = 0.0035 and 0.0069 ridge shapes at α = 8 deg., corresponding to the flow visualization data in Fig. 17. Since a single component hot-wire is not capable of indicating flow direction, the data close to the wall (n/k = 0 in Figs. 18 and 19) must be carefully interpreted. For the k/c = 0.0035 case (Fig. 18), the mean and RMS velocity profiles at x/c = 0.163 were measured immediately downstream of the ridge. The remaining profiles, at progressive downstream locations are consistent with an attached, developing turbulent boundary layer. For the larger ridge (cf. Fig. 19), the

RMS velocity profiles indicate a significant departure from the airfoil surface of the shear layer downstream of the ridge. The magnitude of the peak RMS velocities are much larger for the larger ridge further indicating the fundamentally unsteady nature of the separation region formed downstream of this shape. This is very different from the small-ridge case where the shear layer remains close to the surface as indicated by the RMS velocity profiles. Several of the mean velocity profiles downstream of the larger ridge have an inflection point consistent with separated flow in this region. These measurements together with the surface pressure and flow visualization data indicate a large separation zone for the tall ridge and minimal flow disturbance for the short ridge.

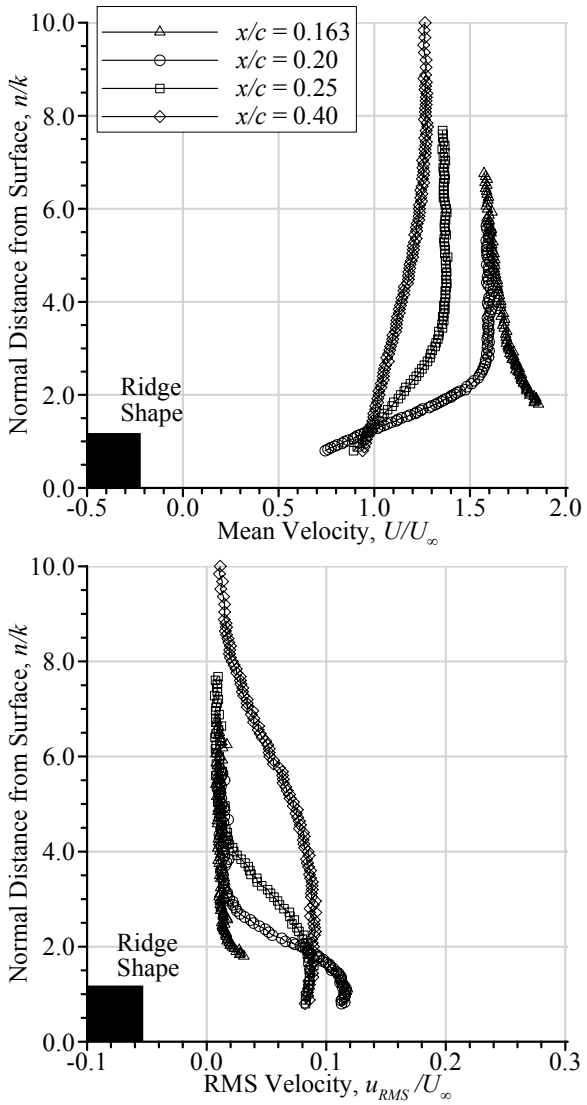

Fig. 18 Mean and RMS velocity profiles downstream of $k/c = 0.0035$ square-cylinder ridge shape located at $x/c = 0.16$ on the NACA 3415 airfoil with $\alpha = 8$ deg., $Re = 1.8\times10^6$, $M = 0.18$, adapted from Whalen.[33]

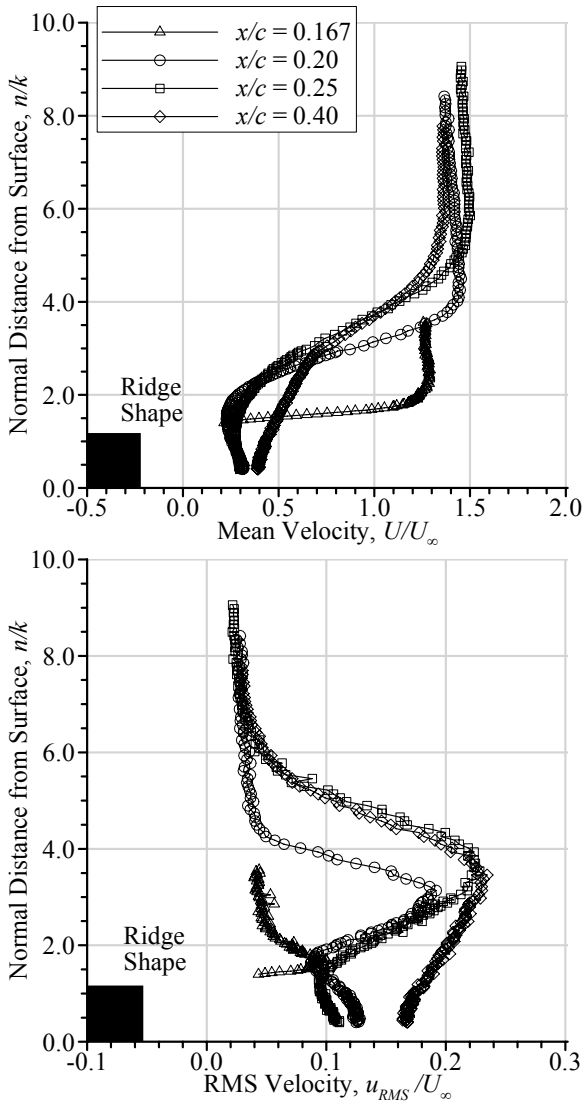

Fig. 19 Mean and RMS velocity profiles downstream of $k/c = 0.0069$ square-cylinder ridge shape located at $x/c = 0.16$ on the NACA 3415 airfoil with $\alpha = 8$ deg., $Re = 1.8\times10^6$, $M = 0.18$, adapted from Whalen.[33]

The chordwise location of upper-surface spanwise ridges is known to have a significant effect on the aerodynamics. With respect to the present discussion, the chordwise location can influence what is classified as a short or tall spanwise ridge. Whalen[33] studied this effect for the $k/c = 0.0035$ square-cylinder shape on the NACA 3415 airfoil. The effect on pressure distribution is shown in Fig. 20 for two locations. The baseline location was $x/c = 0.16$, where the shape is clearly classified as "short." Locating the same artificial ice shape at $x/c = 0.06$ had the effect of significantly altering the pressure distribution. Thus, the same geometry had characteristics of a tall spanwise ridge when located farther forward on the airfoil. The corresponding lift data indicated a significant reduction in maximum lift coefficient and stalling angle of attack relative to the clean configuration at the same Reynolds and Mach number. This stands in contrast to the lift enhancement due to the same artificial ice shape located at the downstream location, $x/c = 0.16$. This effect of chordwise location is consistent with the short-spanwise ridge studies of Calay et al.[4] and Papadakis et al.[5] where lift enhancements were observed for downstream locations while the upstream locations resulted in significant degradations. The effect of chordwise location is driven by a number of factors, such as boundary-layer thickness. The airfoil boundary layer is generally thinner near the leading edge (depending on the transition location), so that even relatively short ridges are many times larger than the local boundary-layer thickness. This and other factors can result in a larger separation bubble downstream of the ridge, which in turn results in a larger effect on the surface pressure distribution and larger performance degradations.

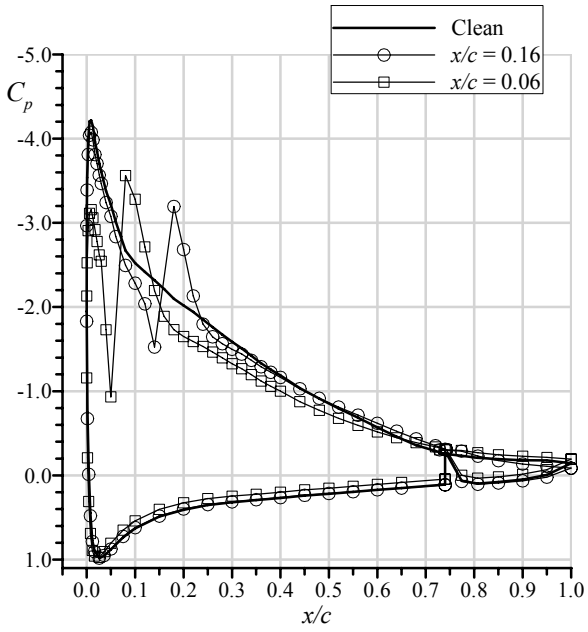

Fig. 20 Surface pressure effect of $k/c = 0.0035$ square-cylinder spanwise-ridge chordwise location on the upper surface of the NACA 3415 airfoil at $\alpha = 12$ deg. , $Re = 1.8\times10^6$, $M = 0.18$, adapted from Whalen.[33]

IV. Conclusions

This paper presents the results of recent investigations into the aerodynamics of simulated runback ice accretion on airfoils. Aerodynamic testing was performed on a full-scale model using a high-fidelity, ice-casting simulation at near-flight Reynolds number. In addition, follow-on subscale testing was conducted with low-fidelity simulations on a quarter-scale model at low-Reynolds number. The high-fidelity, ice-casting simulation was attached to the leading edge of a 72-inch (1828.8-mm) chord NACA 23012 airfoil model and aerodynamic performance measurements were carried out over a Reynolds number range of 4.7×10^6 to 16.0×10^6 and a Mach number range of 0.10 to 0.28. For $Re = 16.0\times10^6$ and $M = 0.20$, the simulated runback ice accretion on the airfoil decreased the maximum lift coefficient from 1.82 to 1.51 and decreased the stalling angle of attack from 18.1 deg. to 15.0 deg. The pitching-moment slope was also increased and the drag coefficient was increased by more than a factor of two. In general, the performance effects were insensitive to Reynolds and Mach number changes over the range tested. While these aerodynamic penalties are significant, they are generally less than the penalties associated with full-scale, high-fidelity, leading-edge ice simulations, including roughness, on the NACA 23012 airfoil.

The results from the full-scale tests were used to evaluate subscale simulation methods for runback ice accretion. Aerodynamic testing was conducted on a quarter-scale NACA 23012 model (18-inch (457.2-mm) chord) at $Re = 1.8\times10^6$ and $M = 0.18$, using low-fidelity, geometrically-scaled simulations of the full-scale casting. It was found that simple, two-dimensional simulations of the upper and lower-surface runback ridges provided the best representation of the full-scale, high-Reynolds number aerodynamics with the ice casting simulation. This adequately simulated the full-scale, iced-airfoil aerodynamics, with the exception of the stall characteristics. A higher-fidelity simulation of the runback ice accretion that included geometrically scaled three-dimensional features resulted in larger performance degradations than what was measured on the full-scale model. The fact that the aerodynamic performance of the airfoil with the subscale simulations is very sensitive to the geometric details such as the addition of surface roughness implies that Reynolds number effects below $Re = 4.7\times10^6$ may not be negligible for this type of ice accretion. An exact scale model of the NG0671 casting was not tested on the subscale model; nor

was an exact scale model of the simple-geometry ridges tested on the full-scale model. This represents a Reynolds number gap between $Re = 1.8\times10^6$ and 4.7×10^6, and a knowledge gap in our understanding of runback-ridge aerodynamics. Furthermore, an alternative scaling length for the runback ice accretion investigated in this report may be required for accurate simulation at Reynolds numbers lower than 1.8×10^6. Future investigations of aerodynamic scaling should consider Reynolds number and perhaps parameters related to the unique behavior of a given airfoil (e.g., pressure gradient) in addition to the geometric scale considered in this work.

The results of this investigation were used to develop a new subclassification of spanwise-ridge ice that distinguishes between short and tall ridges. This subclassification is based upon the flowfield and resulting aerodynamic characteristics, regardless of the physical size of the ridge and the ice-accretion mechanism. Tall spanwise ridges have a profound effect on the airfoil flowfield with a large (and often unsteady) separation bubble that grows rapidly with angle of attack precipitating the stall at low lift coefficient and angle of attack. In contrast, short spanwise ridges are characterized by a small, stable separation bubble formed in the immediate vicinity of the ridge. This small separation zone results in a limited effect on the airfoil flowfield and pressure distribution relative to the clean configuration. The results from this study indicate that more research is required to determine the appropriate aerodynamic simulation methods for short ridges, particularly for Reynolds numbers less than 1.8×10^6.

Acknowledgements

This work was funded by the Federal Aviation Administration (FAA) Office of Aviation Research. While at the University of Illinois, the authors were supported under FAA grant DTFA 96-G-023, with Jim Riley as the contracting officer's technical representative. Additional support, including the use of wind-tunnel models and ancillary equipment, was provided by the NASA Glenn Research Center. This support is gratefully acknowledged.

References

[1]Bragg, M.B., Broeren, A.P., Addy, H.E., Jr., Potapczuk, M., Guffond, D., and Montreuil, E., "Airfoil Ice-Accretion Aerodynamics Simulation," AIAA Paper 2007-0085, Jan. 2007.

[2]Bragg, M.B., Broeren, A.P., and Blumenthal, L.A., "Iced-Airfoil Aerodynamics," *Progress in Aerospace Sciences*, Vol. 41, No. 5, Jul. 2005, pp. 323-418.

[3]Gray, V.H., and von Glahn, U.H., "Effect of Ice and Frost Formations on Drag of the NACA 65_1-212 Airfoil for Various Models of Thermal Ice Protection," NACA TN-2962, June 1953.

[4]Calay, R.K, Holdo, A.E., Mayman, P., and Lun, I., "Experimental Simulation of Runback Ice," *Journal of Aircraft*, Vol. 34, No. 2, Mar.-Apr. 1997, pp. 206-212.

[5]Papadakis, M., and Gile-Laflin, B.E., "Aerodynamic Performance of a Tail Section with Simulated Ice Shapes and Roughness," AIAA Paper 2001-0539, Jan. 2001.

[6]Lee, S., and Bragg, M.B., "Experimental Investigation of Simulated Large-Droplet Ice Shapes on Airfoil Aerodynamics," *Journal of Aircraft*, Vol. 36, No. 5, Sept.-Oct. 1999, pp. 844-850.

[7]Lee, S. and Bragg, M.B., "Investigation of Factors Affecting Iced-Airfoil Aerodynamics," *Journal of Aircraft*, Vol. 40, No. 3, May-June 2003, pp. 499-508.

[8]Broeren, A.P., Lee, S., LaMarre, C.M., and Bragg, M.B., "Effect of Airfoil Geometry on Performance with Simulated Ice Accretions, Vol. 1: Experimental Investigation," Federal Aviation Administration, Washington, D.C., Office of Aviation Research, DOT/FAA/AR-03/64, Aug. 2003.

[9]Whalen, E.A., Broeren, A.P. and Bragg, M.B., "Aerodynamics of Scaled Runback Ice Accretions," *Journal of Aircraft*, Vol. 45, No. 2, Mar.-Apr. 2008, pp. 1076-1088.

[10]Whalen, E.A., Broeren, A.P., and Bragg, M.B., "Considerations for Aerodynamic Testing of Scaled Runback Ice Accretions," AIAA Paper 2006-0260, Jan. 2006.

[11]Broeren, A. P., and Bragg, M. B., "Effect of Airfoil Geometry on Performance with Simulated Intercycle Ice Accretions," *Journal of Aircraft*, Vol. 42, No. 1, Jan.–Feb. 2005, pp. 121–130.

[12]Busch, G.T., Broeren, A.P., and Bragg, M.B., "Aerodynamic Fidelity of Subscale, Two-Dimensional Ice Accretion Simulations," AIAA Paper 2008-7062, Aug. 2008.

[13]Lee, S., Ratvasky, T.P., Thacker, M., and Barnhart, B.P., "Geometry and Reynolds-Number Scaling on an Iced Business-Jet Wing," AIAA Paper 2005-1066, Jan. 2005.

[14]Desplas, P., "F1 Pressurized Subsonic Wind Tunnel User's Guide," Large Technical Facilities, Le-Fauga-Mauzac Wind Tunnels Department, ONERA, France, Nov. 1998.

[15]Allen, H.J., and Vincenti, W.G., "Wall Interference in a Two-Dimensional-Flow Wind Tunnel, with Consideration of the Effect of Compressibility," NACA Report 782, 1944.

[16]Kline, S., and McClintock, F.A, "Describing Uncertainties in Single Sample Experiments," *Mechanical Engineering*, Vol. 75, No. 1, 1953, pp. 3-8.
[17]Coleman, H.W., and Steele, W.G., *Experimentation and Uncertainty Analysis for Engineers*, Wiley-Interscience, New York, 1989, pp. 40-118.
[18]Busch, G.T., "Ice Accretion Aerodynamic Simulation on a Subscale Model," M.S. Thesis, Dept. of Aerospace Eng., Univ. of Illinois, Urbana, IL, 2006.
[19]Blumenthal, L.A., "Surface Pressure Measurement on a Three-Dimensional Ice Shape," M.S. Thesis, Dept. of Aerospace Eng., Univ. of Illinois, Urbana, IL, 2005.
[20]Whalen, E.A., Broeren, A.P., Bragg, M.B., and Lee, S., "Characteristics of Runback Ice Accretions on Airfoils and Their Aerodynamic Effects," AIAA Paper 2005-1065, Jan. 2005.
[21]Whalen, E.A., Broeren, A.P., and Bragg, M.B., "Characteristics of Runback Ice Accretions and Their Aerodynamic Effects," Federal Aviation Administration, Washington, D.C., Office of Aviation Research, DOT/FAA/AR-07/16, Apr. 2007.
[22]Broeren, A.P., Bragg, M.B., Addy, H.E., Jr., Lee, S., Moens, F., and Guffond, D., "Effect of High-Fidelity Ice Accretion Simulations on the Performance of a Full-Scale Airfoil Model," AIAA Paper 2008-0434, Jan. 2008.
[23]Broeren, A.P., Whalen, E.A., Busch, G.T., and Bragg, M.B., "Aerodynamic Simulation of Runback Ice Accretion," Federal Aviation Administration, Washington, D.C., Office of Aviation Research, Report No. to be assigned, 2009.
[24]Busch, G.T., Broeren, A.P., and Bragg, M.B., "Aerodynamic Simulations of a Horn-Ice Accretion on a Subscale Model," *Journal of Aircraft*, Vol. 45, No. 2, Mar.-Apr. 2008, pp. 604-613.
[25]Broeren, A.P., Busch, G.T., and Bragg, M.B., "Aerodynamic Fidelity of Ice Accretion Simulation on a Subscale Model," SAE Paper 2007-01-3285, Sept. 2007. Also published in *SAE 2007 Transactions Journal of Aerospace*, Vol. 116, Sec. 1, Aug. 2008, pp. 560-575.
[26]McCullough, G.B., and Gault, D.E., "Examples of Three Representative Types of Airfoil-Section Stall at Low-Speed," NACA TN-2502, Sept. 1951.
[27]Broeren, A.P., Bragg, M.B., and Addy, H.E., Jr., "Effect of Intercycle Ice Accretions on Aerodynamic Performance," *Journal of Aircraft*, Vol. 41, No. 1, Jan.-Feb. 2004, pp 165-174.
[28]Addy, H.E., Jr., Broeren, A.P., Zoeckler, J.G., and Lee, S., "A Wind Tunnel Study of Icing Effects on a Business Jet Airfoil," AIAA Paper 2003-0727, Jan. 2003, also NASA TM-2003-212124, Feb. 2003.
[29]Addy, H.E., Jr., "Ice Accretions and Icing Effects for Modern Airfoils," NASA/TP-2000210031, also DOT/FAA/AR-99/89, April 2000.
[30]Addy, H.E., Jr., and Chung, J.J., "A Wind Tunnel Study of Icing Effects on a Natural Laminar Flow Airfoil," AIAA Paper 2000-0095, Jan. 2000, also NASA TM-2000-209775, Jan. 2000.
[31]Broeren, A.P., Bragg, M.B., and Addy, H.E., Jr., "Flowfield Measurements About an Airfoil with Leading-Edge Ice Shapes," *Journal of Aircraft*, Vol. 43, No. 4, July-Aug., 2006, pp. 1226-1234.
[32]Kim, H.S., "Effect of Leading-Edge Ice Accretion Geometry on Airfoil Performance," M.S, Thesis, Dept. of Aeronautical and Astronautical Eng., Univ. of Illinois, Urbana, Illinois, 2004.
[33]Whalen, E.A., "Aerodynamics of Runback Ice Accretions," Ph.D. Dissertation, Dept. of Aerospace Eng., Univ. of Illinois, Urbana, IL, 2007.
[34]Tani, I., "Low-Speed Flows Involving Separation Bubbles," *Progress in Aeronautical Sciences*, Vol. 5, No. 2, 1964, pp. 70-103.
[35]Lee, S., Dunn, T., Gurbacki, H., Bragg, M., and Loth, E., "An Experimental and Computational Investigation of Spanwise-Step Ice Shapes on Airfoil Aerodynamics," AIAA Paper 98-0490, Jan. 1998.
[36]Bragg, M., and Loth, E., "Effects of Large-Droplet Ice Accretion on Airfoil and Wing Aerodynamics and Control," Federal Aviation Administration, Washington, D.C., Office of Aviation Research, DOT/FAA/AR-00/14, Apr. 2000.
[37]Lee, S., "Effects of Supercooled Large-Droplet Icing on Airfoil Aerodynamics," Ph.D. Dissertation, Dept. of Aeronautical and Astronautical Eng., Univ. of Illinois, Urbana, IL, 2001.